

Department of Mechanical Engineering Sciences  
Division of Mechanics

ISRN LUTFD2/TFME-22/5044-SE(1-80)

# A molecular dynamics study on the influence of defects on tungsten material properties

Master's thesis by  
**Allan Fredriksson**

Supervisors:

Associate Professor Per Hansson, division of Mechanics, Lund University  
Doctor Leon Petersson, division of Mechanics, Lund University

Examiner:

Professor Aylin Ahadi, division of Mechanics, Lund University

Copyright © 2022 by Allan Fredriksson

Printed by Media-Tryck, Lund, Sweden

For information address:

Division of Mechanics, Lund University, Box 118, SE-211 00 Lund, Sweden

Homepage: <http://www.mek.lth.se>



# Abstract

This masters thesis work has been carried out at the divisions of mechanics at Lund university. The purpose has been to find out more about tungsten and how its material properties are affected by crystal structure defects. This is of interest as tungsten at the research facility ESS will be used in an environment that leads to defects in the material.

Molecular Dynamics (MD), which is a simulation method, will be used in this work for simulating tungsten with different defects. The reason to why these simulations will be performed is that it will increase the understanding of the mechanical behaviour of tungsten. The simulations starts with observing which influence varied variables of sample size, temperature, crystal orientation, potential function, strain rate and boundary condition have on the material properties. This is done in order to choose suitable data input for the final simulations which explores the effect defects like vacancies, vacancy clusters and helium atoms can have on the material properties of tungsten.

From the simulations it emerges that vacancies in a tungsten sample will not affect Young's modulus, but the peak stress and the strain at peak stress will decrease a bit. For this defect the position of the vacancy matters. If this is positioned on a surface, this is worse for the mechanical properties, compared to if it is inside the sample.

Neither vacancy clusters will contribute to a change in Young's modulus. The larger the vacancy cluster, the larger the decrease in the strain at peak stress. The peak stress will not differ this much.

Regarding helium blisters, no risk exists for formation of such on the surface at these temperatures.

Smaller helium clusters inside tungsten can be formed in the environment at ESS, the deterioration of mechanical properties can be quite large due to this.

The risk of larger helium cluster forming in tungsten are small at these temperatures.





# Sammanfattning

Det här examensarbetet har gjorts på mekanikavdelningen på Lunds Tekniska Högskola (LTH) i samarbete med European Spallation Source (ESS). Syftet har varit att undersöka volfram och dess materialegenskaper då kristallstrukturen innehåller defekter. Detta är intressant då volfram på forskningsanläggningen ESS kommer användas i en miljö som leder till defekter i materialet.

Molekylsimulering, som är en simuleringsmetod, kommer att användas i detta arbete för att simulera volfram med olika defekter, dessa simuleringarna kommer att öka förståelsen för materialegenskaperna hos volfram. Simuleringarna startar med att se hur olika storlekar, temperatur, kristallorientering, potentialfunktioner, töjningshastighet och gränsvillkor påverkar materialegenskaperna hos volfram. Dessa resultat kommer att användas som indata till de slutliga simuleringarna som undersöker effekterna som defekter som vakanser, vakanskluster och interstitiella heliumatomer kan ha på volframs materialegenskaper.

Från simuleringarna framkommer det att vakanser inom de givna gränserna inte kommer att påverka E-modulen, men både maxspänningen och töjningen vid maxspänning kommer minska. För denna defekten så har placeringen av vakansen betydelse. Om denna är placerad på en icke-periodisk (fri) yta så är detta sämre för materialegenskaperna än om den befinner sig mitt inne i bulkmaterialet.

Inte heller vakanskluster kommer bidra till någon förändring av E-modulen. Ju större vakanskluster, desto mer minskar töjningen vid brott. Maxspänningen kommer dock ej ändras lika mycket.

Gällande heliumblåsor, vid denna temperaturen finns ingen risk för att dessa kommer att bildas.

Små heliumkluster kan skapas i bulkmaterialet hos volfram, i miljön som råder på ESS, dessa kan försämra de mekaniska egenskaperna ganska mycket eftersom de introducerar inre spänningar i materialet.

Risken att större heliumkluster ska bildas bedöms som väldigt liten vid dessa temperaturer.



# Acknowledgements

This masters thesis project marks the end of my education in mechanical engineering at LTH, Sweden.

The project has been done at the Division of Mechanics in association with the European Spallation Source (ESS).

I would like to give a special thanks to my supervisor Per Hansson and co-supervisor Leon Petersson. They have helped me a lot with valuable advices and comments which have aided me greatly in carrying out this work.

Lund, 18th May 2022.

Allan Fredriksson



# Abbreviations and Explanations

Abbreviations/Explanations	
BC	Boundary condition
BCC	Body-centered cubic
CSP	Centrosymmetry parameter
DFT	Density Functional Theory
EAM	Embedded atom method
ESS	European Spallation Source
FCC	Face-centered cubic
ITER	International Thermonuclear Experimental Reactor
LAMMPS	Large-scale Atomic/Molecular Massively Parallel Simulator.
MC	Monte Carlo
MD	Molecular dynamics
NPT	Constant number of particles, pressure and temperature
NVE	Constant number of particles, volume and energy
NVT	Constant number of particles, volume and temperature
ppp	Periodic BC in all directions.
pps	Periodic BC in x- and y-dir.
pss	Periodic BC in x-dir.
OIS	Octahedral interstitial site
OVITO	Open Visualization Tool
SIA	Self-interstitial atom
TIG	Tungsten inert gas
TIS	Tetrahedral interstitial site
Unit cell	The smallest repeating unit in a crystal structure.



# Contents

Abstract	I
Sammanfattning	III
Acknowledgements	V
Abbreviations and Explanations	VII
Table of Contents	X
<b>1 Introduction</b>	<b>1</b>
1.1 Background	1
1.2 Aim and goal	2
<b>2 Theory, methods and material</b>	<b>3</b>
2.1 Tungsten — the material and its properties	3
2.2 Mechanical properties	5
2.2.1 Stress-strain curve	5
2.2.2 Tensile test	5
2.3 Defects in Tungsten	6
2.3.1 Vacancies	6
2.3.2 Self-interstitial atoms	7
2.3.3 Substitutional atoms	7
2.3.4 Interstitial atoms	7
2.3.5 Dislocations	9
2.4 Computational approach	9
2.4.1 Molecular Dynamics	10
2.4.2 Large-scale Atomic/Molecular Massively Parallel Simulator	15
2.4.3 Interatomic potentials	15
2.4.4 The Embedded Atom Method	16
2.4.5 Visualization and analysis software	18
<b>3 Simulations and results</b>	<b>19</b>
3.1 Potential dependence	19
3.2 Strain rate dependence	21
3.3 Size effects and periodic- compared to non-periodic boundary condition.	22
3.4 Temperature dependence	23
3.5 Influence of crystal orientation	26
3.6 Defect sensitivity	34
3.6.1 Vacancies	34

3.6.2	Vacancy clusters . . . . .	39
3.6.3	Helium atoms in tungsten . . . . .	45
3.6.4	Combination of defects . . . . .	55
<b>4</b>	<b>Conclusions</b>	<b>61</b>
<b>5</b>	<b>Recommendations for future work on the topic.</b>	<b>63</b>
	<b>Bibliography</b>	<b>65</b>
<b>A</b>	<b>Example LAMMPS script</b>	<b>67</b>



# 1 Introduction

## 1.1 Background

The development of new high temperature materials is important in order to meet the demands of future fusion- and fission power generation technology. One promising candidate is tungsten alloys. Still, there are doubts regarding the stability of these alloys under high energy neutron bombardment. Point defects like vacancies and interstitial atoms play an important roll for the microstructural evolution that occurs during irradiation. [1]

Point defects can be created during heat treatments (for example annealing), plastic deformation and irradiation. In metals such as tungsten the formation energy of the vacancies are lower than that of the Self-interstitial atoms (SIA), which means that vacancies are the most usual defect. [2]

The European Spallation Source (ESS) in Lund, will be the world's brightest neutron source facility. A 5 MW proton beam with a duty factor of 4% impinges on a tungsten target [2]. At ESS, protons are accelerated to high velocities and to then collide with a rotating wheel consisting of tungsten blocks. In this collision between protons and tungsten nuclei, high-energy neutrons, which the facility then uses for their experiments, are scattered. Heat and radioactive isotopes are also created during this event, due to this the target is cooled by helium gas and surrounded by a steel structure which shall absorb the unwanted radioactivity. In the collision of the tungsten target, point defects, such as vacancies, can appear. [3]

For ESS the low ductility and a high ductile to-brittle transition temperature of tungsten here pose a challenge.

As mentioned above tungsten is one of the leading candidates as a surface material in fusion reactors. The material properties of tungsten are affected by the plasma and its bi-products. The International Thermonuclear Experimental Reactor (ITER) divertor (in nuclear fusion, a divertor is a device which allows the online removal of waste material from the plasma while the reactor is still operating) contains surfaces of tungsten at a temperature of about 1000K, that are bombarded by low-energy helium ions. About two thirds of these bounce away, while the last third penetrates the surface and reaches mean depths of 1 nm. In the collision that takes place on the surface, the energy lies below the tungsten threshold, which means that no defects are created on the surface due to the impact. The helium atoms that have entered the tungsten material start to diffuse. After a while they form helium clusters inside the tungsten bulk atoms. [4]

Because the density of helium bubbles is relatively low compared to the bulk atoms, the bubbles feel an attraction from the free surface which often results in that the bubble grow towards the surface, in the direction of least resistance. [5]

## 1.2 Aim and goal

The purpose of this thesis has been to find out more about tungsten when it contains defects, which can emerge under the current circumstances at the ESS facility. Molecular dynamics (MD) is the simulation technique used in this work, with this it will be possible to observe which influence varied variables and defects in a tungsten sample, will have on the mechanical properties. Defects chosen to study are vacancies, vacancy clusters and interstitial atoms in the form of helium. The simulations will be performed as described below.

**Vacancies:** A vacancy is a missing atom in the crystalline lattice. For this defect type an input from ESS of atomic vacancies between  $1 * 10^{23}$  and  $1 * 10^{25}$  per  $m^3$  was given. Which impact the position of the vacancy has on the mechanical properties, were also studied.

**Vacancy clusters:** A vacancy cluster is when vacancies are gathered in a group, in this work vacancy cluster sizes up to 128 were placed centrally inside the samples in order to observe if the mechanical properties were affected by these.

**Helium atoms:** For the defect of helium atoms, four different cases will be tested.

- Relaxation of tungsten containing randomly distributed helium atoms, to see how helium clusters are formed. This was tested for 50, 100 and 200 helium atoms at three different temperatures of 300K, 700K and 1000K.
- Formation of helium blisters on a tungsten surface. Here one for the temperatures 700K and 1500K will study what effect a growing helium cluster inside a tungsten sample can have on the tungsten surface.
- Deformation of tungsten containing one centrally placed helium cluster of size 75, 150 and 300 atoms, to see what influence these have on the mechanical properties.
- Deformation of tungsten containing helium clusters randomly distributed over the sample. The aim of this simulation is to see if the small clusters are deteriorating for the material. The number of helium atoms in this simulation will be 200, 400 and 800.

# 2 Theory, methods and material

## 2.1 Tungsten — the material and its properties

A summary of the material properties of tungsten can be found in Table 2.1. As shown here tungsten has the highest melting point of all metals, very high thermal conductivity and its thermal expansion is lowest of all elements. The atomic structure of tungsten can be seen in Figure 2.1. For the last three properties of the table, the data comes from commercially pure tungsten i.e. , material delivered by suppliers for commercial use. In the simulations made in this work where there exist no defects, these values will be very different. This can be seen in the stress-strain curves in the result section.

**Table 2.1:** Material properties of tungsten.

Material properties, units	Values	Comments
Density, ( $kg/m^3$ )	19300 [6, p. 856]	
Melting point, ( $K$ )	3414 [6, p. 32]	Highest of all metals
Atomic number	74 [6, p. 935]	
Atomic mass, (u)	183.84 [6, p. 935]	
Atomic radius, (nm)	0.1371 [6, p. 51]	
Thermal conductivity, ( $\frac{W}{mK}$ )	178 [6, p. 759]	Higher than most metals
Coefficient of linear thermal expansion, ( $\frac{m}{mK}$ )	$4.5 * 10^{-6}$ [6, p. 759]	Lowest of all elements
Atomic structure (below melting point)	BCC [6, p. 51]	See Figure 2.1
Bonding	Metallic [6, p. 32]	
Lattice parameter $a_0$ , ( $\text{\AA}$ )	3.16 [6, p. 53]	See Figure 2.1
Material category	Transition metal [6, p. 27]	
Young's modulus, (GPa)	400 [6, p. 860]	Commercially pure
Yield strength , (MPa)	760 [6, p. 866]	Commercially pure
Tensile strength , (MPa)	960 [6, p. 866]	Commercially pure

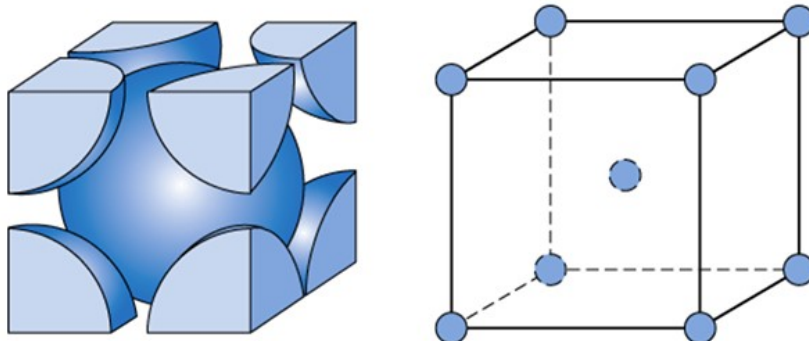


**Figure 2.1:** Body Centered Cubic unit cell, in this structure there are atoms in all eight corners and one in the center of the cube. Side length of unit cell are denoted  $a_0$ . [6, p. 53]

The strong metallic bonding in the tungsten contributes to a large Young's modulus, high strength and hardness. Its resistance to high temperatures has led to that it is used for Tungsten Inert GAS (TIG) welding electrodes and historically for filament in bulbs. Another field of application is in metalforming and metalcutting, where tungsten is used in the shape of tungsten carbides like  $WC$  or  $W_2C$ .

Crystallographic planes are planes that can be defined inside a crystal in which the atomic concentrations are high [6, p. 81].

Dislocations do not move as easy along all crystallographic planes and in all crystal orientations. The plane in which the dislocation motion occurs is called the slip plane, and in this plane there are specific directions in which this motion is moving [6, p. 284]. Tungsten has two different slip planes,  $\{1\ 1\ 0\}$  and  $\{2\ 1\ 1\}$ , see images of these in Figure 2.2

In a slip system slip can occur within the crystallographic plane, in the crystallographic direction. [6, p. 903] Two of the possible slip systems for tungsten can be seen in Figure 2.2.

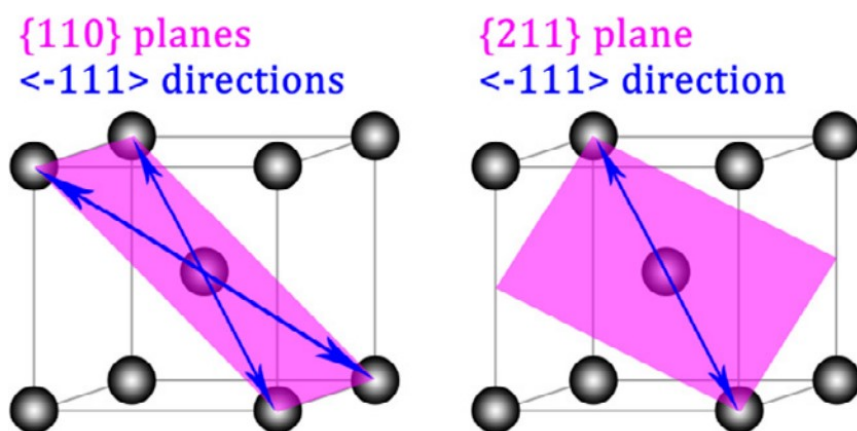


**Figure 2.2:** Main slip systems in tungsten, both of the slip systems have 12 possible configurations. ref [7]

## 2.2 Mechanical properties

### 2.2.1 Stress-strain curve

A stress-strain curve is a curve that gives the relation between stress  $\sigma$  and strain  $\varepsilon$ , Figure 2.3 shows an example of a stress-strain curve. From this curve it is possible to extract Young's modulus as the slope of the tangent line, when the strain is zero.

Young's modulus is the ratio of stress to strain when deformation is totally elastic, it is also a measure of the stiffness of a material. [6, p. 900]

The curve also gives tensile stress, or peak stress, which is the stress at the top of the curve.

Necking is when a small neck begins to form at this stress somewhere at the surface of the sample, this is where the fracture happens. [6, p. 230] When looking at typical stress-strain curve of tungsten free from defects like in Figure 2.3, necking is not existing because the material is so brittle.

In a stress-strain curve the linear part of the stress-strain plot is called the elastic stage. The plastic stage is the deformation that occurs when the stress exceeds the yield stress.

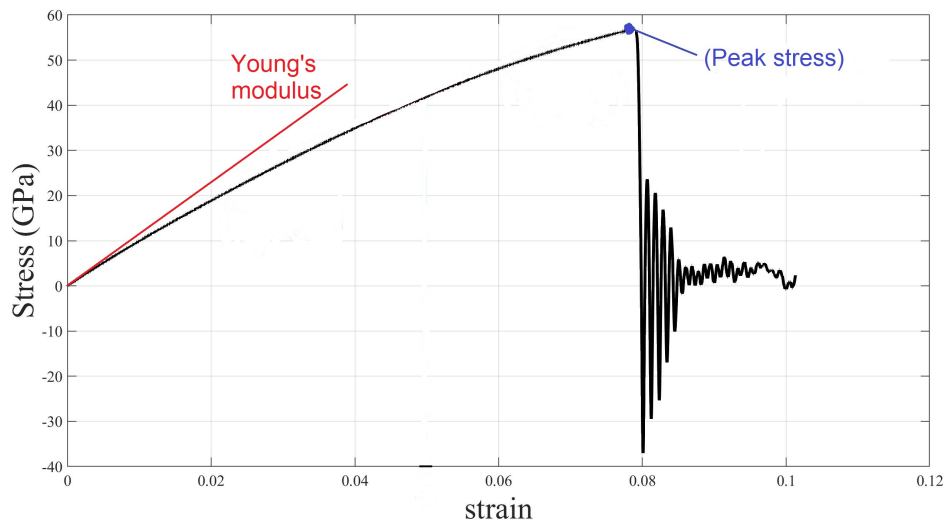


**Figure 2.3:** Example of a stress-strain curve for a tungsten sample with a cross section of 24x24 unit cells. Young's modulus, corresponds to the slope of the tangent line, when the strain is zero. Peak stress are given by the position of the blue dot.

### 2.2.2 Tensile test

An MD simulation of a tensile test may be used in order to determine mechanical properties of materials. The test starts with a relaxation at a certain number of timesteps, where the goal is to minimize the kinetic energy among the atoms within the sample, see Figure 2.4. When the real simulation starts you want a stable system,

or else stresses might be introduced into the system. The next step is to add a constant velocity  $v$  that is applied uniaxially along the long axis of a sample, to simulate a displacement-controlled uniaxial tensile loading. The specimen is then deformed to fracture. The forces between all atoms in the sample parallel to the long axis ( $F_{xx}(n)$ ) are computed every timestep  $n$  throughout the simulation. In an effort to get a mean value of the stress in the long axis direction these computed forces are summed and divided by the total number of atoms  $N$ . This is the stress used in the stress-strain curve, thus

$$\sigma_{xx} = \frac{\sum_{n=1}^N (F_{xx}(n))}{N}. \quad (2.1)$$

The strain at a certain timestep  $n$  is calculated by multiplying the constant velocity  $v$  by the time of the certain timestep  $n$ , and finally divide this by the original length  $L_0$ , as

$$\varepsilon = \frac{\Delta L}{L_0} = \frac{v * t(n)}{L_0}. \quad (2.2)$$

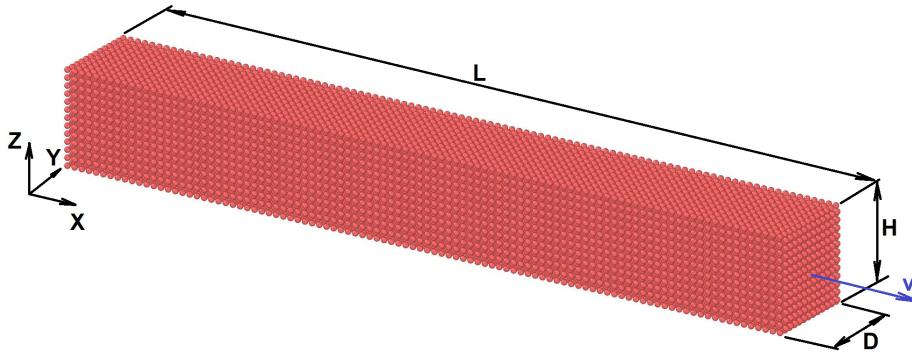


**Figure 2.4:** Computational model of single crystal block of size  $L \times D \times H$  under uniaxial tensile loading in x direction at constant velocity  $v$ .

## 2.3 Defects in Tungsten

### 2.3.1 Vacancies

A vacancy is a missing atom in the crystalline lattice. For this defect type we received input from ESS of atom vacancies between  $1 \times 10^{23}$  and  $1 \times 10^{25}$  per  $m^3$ . Since a  $m^3$  holds  $6,44 \times 10^{28}$  tungsten atoms, this defects corresponds to values between  $1.5529783 \times 10^{-4}$  % and  $1.5529783 \times 10^{-2}$  %. As mentioned by [8], the equilibrium concentration of vacancies  $c$  as a function of the temperature can be calculated as

$$c = e^{\frac{-E_f}{kT}}; \quad (2.3)$$

where  $E_f$  is the vacancy formation for tungsten, 3.3eV [8];  $k$  is Boltzmann constant,  $8.617333262 * 10^{-5} eV/K$  [6, p. 895]; and  $T$  is the absolute temperature, which in our case is 700K. At this temperature the equilibrium concentration of vacancies will be about  $1.74199016 * 10^{-24}$ . Since it is known that a  $m^3$  holds  $6,44 * 10^{28}$  tungsten atoms, this corresponds to vacancies of about  $112184 atoms/m^3$ . The reason this vacancy is so much smaller than the vacancies given earlier in the text must be because at ESS, tungsten is beside the temperature even exposed to high-energy radiation which causes further vacancies.

### 2.3.2 Self-interstitial atoms

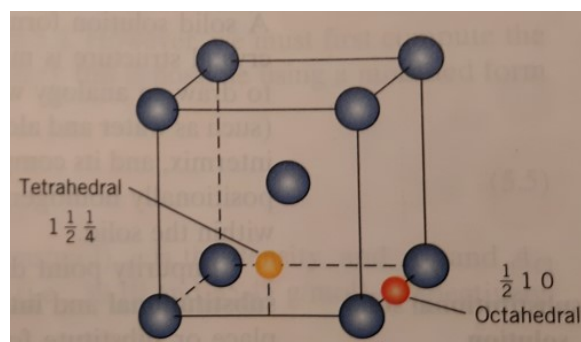
A (SIA) is an atom of the bulk material that has left its position in the crystal and instead is positioned in an interstitial site. Since the atom is larger than the size of the hole, this introduces large distortions of the crystal pattern. This defect is however relatively rare, and exists in concentrations that are lower than for vacancies. [6, p. 148-160]

### 2.3.3 Substitutional atoms

If a host atom is replaced by another of a different material it is called a substitutional atom. Examples of this are tungsten carbides like  $WC$  or  $W_2C$ .

### 2.3.4 Interstitial atoms

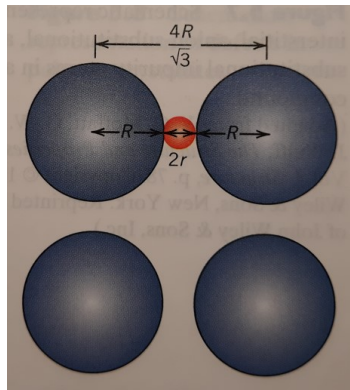
Interstitial atoms are atoms that are placed between the lattice host atoms. In tungsten, which has a BCC structure, there exists two types of interstitial spaces, tetrahedral and octahedral, as shown in Figure 2.5. Metallic materials such as tungsten have a high packing factor, this means that interstitial sites are relatively small. As a consequence of this, the interstitial atoms have to be smaller than the bulk atoms. [6, p. 148-160]



**Figure 2.5:** The two types of interstitial positions existing for tungsten. The blue spheres represents the tungsten atoms and the yellow and red spheres marks where the interstitial atoms can be positioned. [6, p. 154]

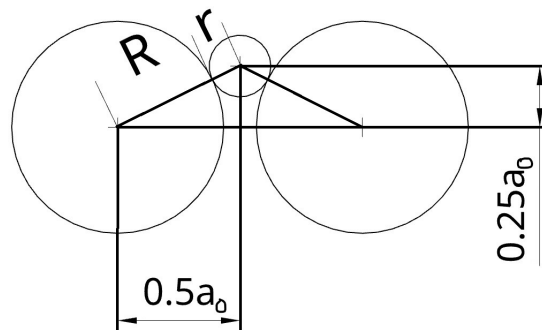
Now the the largest possible radiuses of both interstitial spaces seen in Figure 2.5 will be calculated. The Octahedral Interstitial Site (OIS) will be calculated first.

Figure 2.6 gives the needed geometry to calculate the largest possible OIS radius, without introducing stresses into the lattice. The sidelength of the unit cell can be expressed as  $2R+2r$ , this must be equal to  $\frac{4R}{\sqrt{3}}$  [6, p. 53], solving this equation gives that  $r = 0.155R$ , here  $r$  is the interstitial atomic radius and  $R$  is the host atomic radius. The atomic radius for tungsten is 137.1 pm, this gives us a possible OIS radius of  $r = 21.25$  pm. This radius is smaller than all atomic radiuses in the periodic system, this means that stresses are built into the lattice if any atom is placed in an OIS position.



**Figure 2.6:** BCC structure with an interstitial atom. The blue spheres marks the tungsten atoms, while the red one is a OIS atom. [6, p. 155]

After this the largest possible radius of the Tetrahedral Interstitial Site (TIS), without introducing stresses into the lattice, will be calculated. By looking at how this interstitial is positioned inside the unit cell in Figure 2.5 , a simple sketch of the geometry can be made, as has been done in Figure 2.7 .



**Figure 2.7:** BCC structure with an interstitial atom. The larger spheres marks the tungsten atoms, while the little one is a TIS atom.

As shown in Figure 2.6 the sidelength of the unit cell is  $a_0 = \frac{4R}{\sqrt{3}}$  [6, p. 155]. This in combination with using Pythagoras theorem for the geometry in Figure 2.7 gives the following equation system

$$\begin{cases} a_0 = \frac{4R}{\sqrt{3}} \\ (R + r)^2 = (\frac{1}{4}a_0)^2 + (\frac{1}{2}a_0)^2 \end{cases}$$

this can be rewritten as



$$\begin{cases} R = \frac{\sqrt{3}a_0}{4} \\ r = a_0\left(\frac{\sqrt{5}}{4}\right) - R \end{cases}$$

which gives the ratio

$$\left\{ \frac{r}{R} = \frac{\sqrt{5}-\sqrt{3}}{\sqrt{3}} = 0.291 \right.$$

Inserting the atomic radius 137 pm of tungsten into this equation gives the largest possible radius  $r=39.9$  pm of the TIS. Materials with atomic radius smaller than this can diffuse as interstitial atoms without introducing strains in the host lattice. Example of possible interstitial atoms are hydrogen (radius 37pm [9]) and helium (radius 31pm [9]), in this work only helium atoms will be considered.

Helium atoms are most of the time positioned in the tetrahedral sites. When the kinetic energy of a helium atom is high enough the atom can execute several jumps from TIS to TIS in a short time. These jumps appear to have ballistic characteristics. When temperature increases the jumps occur more often and jumps from one TIS can pass through an OIS. [10]

### 2.3.5 Dislocations

A dislocation is a linear defect in a crystal structure where there exist atomic misalignment. Plastic deformation corresponds to the motion of dislocations in response to an applied shear stress. Examples of dislocations are edge, screw and mixed dislocations. [6, p. 896]

Edge dislocation is a defect in which an extra half-plane of atoms is introduced inside the crystal, this distorts the surrounding atom planes. The dislocation line is perpendicular to Burgers vector. [6, p. 897]

Screw dislocation is a defect that unzips the lattice when moving through it, creating a screw. The Burgers vector is parallel to the dislocation line.[6, p. 903]

Mixed dislocation is a defect that has both edge- and screw components.[6, p. 900]

Lack of time causing that no simulations regarding dislocations will be brought up in this work.

## 2.4 Computational approach

Many types of computer-driven atomistic simulations exist, Molecular Dynamics (MD), Monte Carlo (MC) and Density Functional Theory (DFT) are some of the most common. [11]

MD is a simulation method for analyzing the physical movements of atoms. MD uses the physical positions of atoms and by solving the equation of motions, the forces between them are known.

MC uses randomness to solve complex or nonlinear problems. With DFT one can

prove that the energy of a system of atoms is given exactly by a functional of its electronic density. [12]

In this work MD will be used.

For computational reasons it is necessary to restrict the size of the sample that will represent the whole system which should be analyzed in the MD simulation. This means that the ratio between the number of surface atoms and the total number of atoms will differ from the real value of the system. In small samples a higher proportion of the atoms will be located on the surface, and thus have fewer neighbors than the bulk atoms. In a simulation these surface effects would not be in proportion to the real ones. For this reason periodic boundary conditions are preferable in large systems. Periodic boundary conditions means that the atoms are packed into a box, which is surrounded by translated copies of itself. This will reduce surface effects and as a result the simulation will emulate bulk properties. [13]

Before a simulation can get started, an assumption [13] has to be made: Since the mass of the atomic nucleus is so much larger than the electrons, it is assumed to be the interacting material point. For each of these particles, position- and velocity vectors are calculated to describe their motion.

### 2.4.1 Molecular Dynamics

Molecular Dynamics is a computer simulation method that simulates the motion of atoms according to Newton's laws of motion. The atoms are approximated as balls on springs. An MD simulation starts with calculating the forces on all atoms, Newton's second law then gives the accelerations of all atoms. By integrating Newton's equations of motion one gets the new positions of the atoms. After this the time is updated by adding a time step. This process is repeated until the end of the simulation.

A molecular dynamics procedure can be described by the steps shown in Figure 2.8.

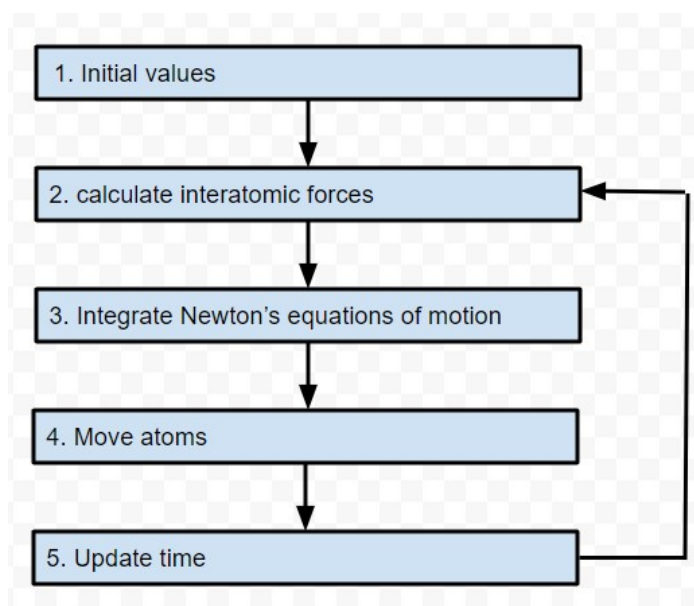


**Figure 2.8:** Scheme of the molecular dynamics simulation procedure.

## 1. Data input

One has to define:

- **Boundary conditions.**

BC is a description of how the boundaries of the simulation box shall be treated during the simulation. BC:s must be specified both for the lower and upper face of the simulation box three dimensions. S stands for non-periodic, p stands for periodic. Periodic boundary conditions means that the atoms are packed into a box, which is surrounded by translated copies of itself. This will better emulate bulk properties compared to non-periodic boundary conditions. Boundary conditions used in this work is pss, pps and ppp.

- **The lattice parameter.**

Lattice parameter  $a_0$  is the side length of the unit cell.

- **The potential function.**

The potential function is a description of how the particles in the simulation will interact.

- **The mass of the atoms.**

- **The crystal structure.**

- **The crystal orientation inside the sample.**

A crystal orientation can be thought of as the direction in which a crystal grows relative to the coordinate system of the sample. In this work three different orientations have been dealt with,  $[1\ 0\ 0]$ ,  $[1\ 1\ 0]$  and  $[1\ 1\ 1]$ .

- **The physical dimensions of the geometry which is desired to be examined has to be stated.**

- **The temperature.**

- **Statistical ensemble.**

As a part of the simulation parameters a choice has to be made by four different set of thermodynamic variables also called statistical ensembles. These are NVE(Microcanonical ensemble), NVT(Canonical ensemble), NPT(Isothermal–isobaric) and NPH(Isoenthalpic–isobaric).

Here N stands for number of particles, V for volume, E for internal energy, T for temperature, P for pressure and H for enthalpy [14]. The mentioned properties can be specified and kept constant throughout the simulation.

In this work NVT and NPT will be used.

- **Number of timesteps.**

- **The timestep.**

The timestep is a very important parameter of a MD simulation and choosing it correctly will be a balancing act between numerical precision and simulation time. The shorter the timestep the more realistic the simulation, but the longer the computing time. If timestep is too large it may lead to atoms overshooting

their expected positions. This can be avoided with timesteps short enough to capture atomic vibrations, because updating of the positions and trajectories happens more often here. Here, a time step of 5fs is chosen after performing several simulations with different timesteps of tungsten samples at temperature 700K. From Figure 2.9 one can clearly see that with this timestep, the stress converges almost to zero during the relaxation, which lasts for 50000 timesteps.

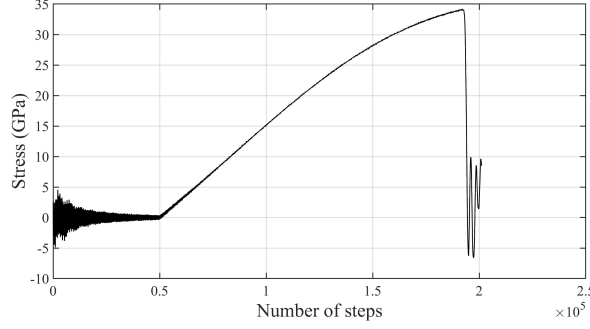


**Figure 2.9:** Stress as a function of step numbers. Here the timestep=5fs.

This work includes simulations of tungsten with interstitial atoms, but since the mass of helium atoms is much smaller than tungsten atoms one can not use the same timestep as in pure tungsten simulations. The first step in computing this periodic time is to consider a system of two atoms with a force acting between them as a harmonic oscillator, see Figure 2.10

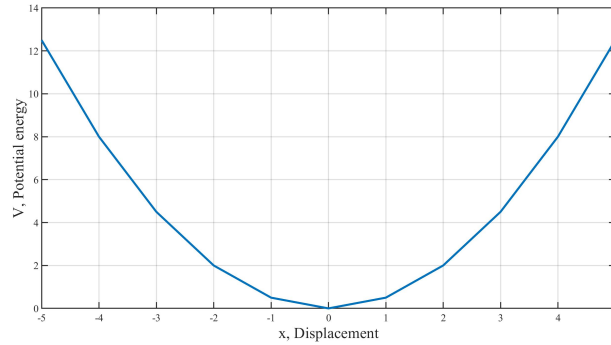


**Figure 2.10:** Harmonic oscillator, here  $x$  can be seen as the position of an atom in a potential well formed by a crystal lattice. The equilibrium position is given by  $x=0$ .

Newton's second law for a oscillating motion

$$m\ddot{x} = -kx, \quad (2.4)$$

which is equivalent to

$$\ddot{x} + \frac{k}{m}x = 0. \quad (2.5)$$

Here  $k$  is a constant and  $x$  and  $m$  are the position and mass of the body. Introducing the frequency  $\omega_n$  as

$$\omega_n^2 = \frac{k}{m}, \quad (2.6)$$

the solution can be written on the periodic form

$$x = A\cos(\omega_n t) + B\sin(\omega_n t). \quad (2.7)$$

The period is

$$T_n = \frac{2\pi}{\omega_n}. \quad (2.8)$$

In order to get the ratio of the periodic time between helium and tungsten, Equation (2.6) is used in combination with (2.8).

$$ratio_{He} = \frac{\sqrt{m_{He}}}{\sqrt{m_W}} \quad (2.9)$$

Thus the timestep for helium will be  $ratio_{He}$  times the timestep for pure tungsten.

If atomic masses of tungsten and helium are inserted into equation 2.9, a value of 0.1475 is received. This means that the timestep when simulating helium atoms, needs to be about 1/7 compared to the value of tungsten. A time step of 1 fs is chosen for these simulations.

## 2. Calculation of the interatomic forces

The force acting on atom  $i$  will be calculated by using the interatomic potentials.

$$\mathbf{F}_i = -\nabla_i V(\mathbf{r}_1, \dots, \mathbf{r}_n), \quad (2.10)$$

where  $V(\mathbf{r}_1, \dots, \mathbf{r}_n)$  is the potential energy function;  $i$  is a number between 1 and  $n$ , where  $n$  is the total number of atoms; and the gradient with respect to atom  $i$ ,  $\nabla_i$  is defined as

$$\nabla_i = \begin{pmatrix} \frac{\partial}{\partial x_i} \\ \frac{\partial}{\partial y_i} \\ \frac{\partial}{\partial z_i} \end{pmatrix}, \quad (2.11)$$

where  $[x_i, y_i, z_i]$  is the position of atom  $i$ .

Equation 2.10 will hereafter be used to obtain the force  $\mathbf{F}_i$  working on each atom.

This force can by Newton's second law give the acceleration  $\mathbf{a}_i$  of the  $i$ th atom

$$\mathbf{a}_i = \frac{\mathbf{F}_i}{m_i}, \quad (2.12)$$

where  $m_i$  is the mass of the  $i$ th atom. This equation provides the acceleration at the time  $t$ . Now the initial position, velocity and acceleration for all  $n$  atoms are known, this means that the goal of solving the equation of motion is within reach.

### 3. Integrate Newton's equations of motion

MD uses Newton's second law,

$$\mathbf{F}_i = m_i \mathbf{a}_i = m_i \frac{\partial \mathbf{v}(t_0)}{\partial t} = m_i \frac{\partial^2 \mathbf{r}(t_0)}{\partial t^2}, \quad (2.13)$$

to calculate the trajectories of atoms.

The first step will be to find position, velocity and acceleration at time  $t + \Delta t$  and  $t - \Delta t$ . Start with getting the coordinates. We can expand the position around the time  $t$  as

$$\begin{aligned} \mathbf{r}(t - \Delta t) &= \mathbf{r}(t) + \sum_{k=1}^{\infty} \frac{1}{k!} \frac{\partial^k \mathbf{r}(t)}{\partial t^k} (-\Delta t)^k \\ \mathbf{r}(t + \Delta t) &= \mathbf{r}(t) + \sum_{k=1}^{\infty} \frac{1}{k!} \frac{\partial^k \mathbf{r}(t)}{\partial t^k} \Delta t^k. \end{aligned} \quad (2.14)$$

If equations in 2.14 are expanded to the third order, velocity  $\mathbf{v}(t)$  and acceleration  $\mathbf{a}(t)$  will appear along with the third-order position derivative  $\mathbf{b}(t)$ , giving

$$\begin{aligned} \mathbf{r}(t - \Delta t) &= \mathbf{r}(t) - \frac{\partial \mathbf{r}(t)}{\partial t} \Delta t + \frac{1}{2} \frac{\partial^2 \mathbf{r}(t)}{\partial t^2} \Delta t^2 - \frac{1}{6} \frac{\partial^3 \mathbf{r}(t)}{\partial t^3} \Delta t^3 + \frac{1}{24} \frac{\partial^4 \mathbf{r}(t)}{\partial t^4} \Delta t^4 \\ \mathbf{r}(t + \Delta t) &= \mathbf{r}(t) + \frac{\partial \mathbf{r}(t)}{\partial t} \Delta t + \frac{1}{2} \frac{\partial^2 \mathbf{r}(t)}{\partial t^2} \Delta t^2 + \frac{1}{6} \frac{\partial^3 \mathbf{r}(t)}{\partial t^3} \Delta t^3 + \frac{1}{24} \frac{\partial^4 \mathbf{r}(t)}{\partial t^4} \Delta t^4. \end{aligned} \quad (2.15)$$

This is the same as

$$\begin{aligned} \mathbf{r}(t - \Delta t) &= \mathbf{r}(t) - \mathbf{v}(t) \Delta t + \frac{1}{2} \mathbf{a}(t) \Delta t^2 - \frac{1}{6} \mathbf{b}(t) \Delta t^3 + O(\Delta t^4) \\ \mathbf{r}(t + \Delta t) &= \mathbf{r}(t) + \mathbf{v}(t) \Delta t + \frac{1}{2} \mathbf{a}(t) \Delta t^2 + \frac{1}{6} \mathbf{b}(t) \Delta t^3 + O(\Delta t^4). \end{aligned} \quad (2.16)$$

Adding the two expressions in 2.16 gives

$$\mathbf{r}(t + \Delta t) = 2\mathbf{r}(t) - \mathbf{r}(t - \Delta t) + \mathbf{a}(t) \Delta t^2 + O(\Delta t^4), \quad (2.17)$$

which is the basic form of the Verlet time integration algorithm; which is used by many MD simulators because of its simplicity, accuracy and stability. [13]

The position and velocity are given as a function of time by integrating equation 2.13. The acceleration is obtained in the same way as before, i.e. the forces are calculated from the new positions, allowing the acceleration to be obtained by using equation

(2.12). Equation 2.17 now gives the positions of the atoms at time  $t + \Delta t$ , and as can be seen there are no need of the velocities in order to update the position.

#### 4. Move atoms

The atoms are moved to new positions given by Equation 2.17.

#### 5. Update time

The time is now updated by adding one timestep,  $t \rightarrow t + \Delta t$

Now move back to step 2 again and this process is repeated until the end of the simulation. [15]

### 2.4.2 Large-scale Atomic/Molecular Massively Parallel Simulator

LAMMPS [16] is used to propagate the system in this work. LAMMPS is a classical molecular dynamics code that can be run on either a single processor or parallel on several processors. LAMMPS was developed in the middle of the 1990s, but had its real breakthrough first in year 2004 when the source code was released. [17]

In Appendix A an example of a LAMMPS input script can be found.

This program firstly defines a sample size of 100x24x24 unit cells, consisting of tungsten atoms with crystal direction [1 0 0], and has a lattice parameter 3.14339Å.

The temperature is 700K.

The potential function is EAM4.

Time step length is 5fs.

Boundary conditions are pss.

This simulation starts with performing a relaxation process consisting of 50000 time steps. Thereafter it performs a tensile test where the strain rate is  $1 \times 10^8/s$ . Here there are 500000 time steps. The screen output every 50 time steps will be: step number, current length, volume, temperature, stress in x-direction, strain.

### 2.4.3 Interatomic potentials

The interatomic potential function describes how the atoms interact. This function is a list of the potential energy for the whole system at many possible positions of the atomic nucleus. The potential energy function can be written as

$$V(\vec{r}_1, \dots, \vec{r}_n) = V_1 + V_2 + V_3; \quad (2.18)$$

where  $V_1$  is the energy due to an external force field, like gravity or electrostatic, but in most cases this is overlooked,  $V_2$  represents pair-wise interactions of the particles, and  $V_3$  is the three-body component, which often is included in  $V_2$  to make the calculations easier.

Pair-wise interaction means that two-by-two atoms are considered, while many-body interactions refer to larger system than two atoms.

An example of a potential that takes many-body interactions (collective behaviour of multiple atoms interacting) into consideration is the Embedded Atom Method (EAM) potential which computes the electron density with help from the positions of nearby atoms. [12]

A neighbor list contains information about the positions of atoms in relation to each other, with respect taken to boundary conditions. This list may be invalidated when atoms are moved, therefore a method is used which checks if it is still valid, and updates it if not. [18]

To reduce calculation time a cut-off radius  $r_{cut}$  is introduced. The pair-wise interactions of the atoms will only be calculated if the distances from the center of one atom to another is smaller or equal to  $r_{cut}$ . This will reduce the neighbor numbers without affecting the energy much, since the forces between the atoms are close to zero over this distance. This gives the form

$$V(r) = \begin{cases} \phi(r) - \phi(r_{cut}) & \text{if } r \leq r_{cut} \\ 0 & \text{if } r > r_{cut} \end{cases} . \quad (2.19)$$

There are many potentials, two of the most common ones being the EAM and the Lennard-Jones (LJ) potential. The LJ potential which only considers atoms two-by-two, works good to describe properties of gases and fluids, but in the case of covalent- or metallic bonds it's not very accurate. The properties predicted by an atomistic simulation are only as good as the quality of the underlying interatomic potential. In this work EAM potentials will be used, these will be described more thoroughly in next paragraph.

#### 2.4.4 The Embedded Atom Method

EAM potentials are a type of interatomic potential mainly used in metallic systems. This potential describes each atom as embedded in a host electron gas created by the surrounding atoms. The amount of energy needed to insert one atom into the electron gas of a given density is called the embedded function, which deals with multi-atom effects. This potential can be used for example when examining fracture and defects of metals. [13]

The good thing about EAM is that it only requires only 2-5 times the work of a pair-potential model (like LJ potential), yet includes some many-body effects that are important for the description of metallic systems. [12]



The total energy  $E_{tot}$  of a system of N atoms can be written as a sum over atom energies [12],

$$E_{tot} = \sum_i^N E_i. \quad (2.20)$$

The potential energy of an atom i, can be described by ref [12]

$$E_i = F_\alpha \left( \sum_{i \neq j} \rho_\beta(r_{ij}) \right) + \frac{1}{2} \sum_{i \neq j} \phi_{\alpha\beta}(r_{ij}), \quad (2.21)$$

where F is the embedding energy required to place atom i of type  $\alpha$  into the electron cloud,  $\rho_\beta$  is the contribution to the electron charge density from atom j of type  $\beta$  at the location of atom i,  $r_{ij}$  is the distance between atoms i and j, and  $\phi_{\alpha\beta}$  is a pair-wise potential function. For systems consisting of only one type of atom, three mathematical relations have to be specified. The embedding function, a pair-wise function and the electron cloud contribution function. [13]

The way to calculate the EAM energy is much the same as for a pair-potential model. For atom i, the sums of  $\rho_\beta(r_{ij})$  and  $\phi_{\alpha\beta}(r_{ij})$  are calculated for neighbors j, and thereafter  $F_\alpha \left( \sum_{i \neq j} \rho_\beta(r_{ij}) \right)$  is calculated. [12]

It is possible to assume that  $\sum_{i \neq j} \rho_\beta(r_{ij})$  is a measure of a local atomic density close to atom i. This assumption requires that  $\rho_\beta(r_{ij})$  is a function that decreases when  $r_{ij}$  increases. The assumption means that EAM can be seen as a potential consisting of the sum the pair potential over the whole volume, (pair potentials are defined between pairs of atoms that are within the cutoff radius). This approach takes defects, like free surfaces into consideration. The fundamental benefit of EAM is the nonlinearity of the term  $F_\alpha \left( \sum_{i \neq j} \rho_\beta(r_{ij}) \right)$ , this gives a many-body contribution to the energy.  $\sum_{i \neq j} \rho_\beta(r_{ij})$  is only depending on distances to neighboring atoms, thus the many-body term has no angular dependence. [12]

In brief, the contents of EAM can be said to be:  $\rho_\beta(r_{ij})$  which is the electronic density as a function of distance from the center of the atom,  $\sum_{i \neq j} \rho_\beta(r_{ij})$  which corresponds to the density of the host system with atom i removed,  $F_\alpha \left( \sum_{i \neq j} \rho_\beta(r_{ij}) \right)$  which is the quantum mechanical energy of the embedded atom i within a homogeneous electron gas with density  $\rho_\beta(r_{ij})$ , and finally  $\phi_{\alpha\beta}(r_{ij})$  which is the classical electrostatic interaction between atoms i and j. [11]

One good way to illustrate the predictive power of EAM is to examine what happens at free surfaces during a relaxation procedure. At a free surface the atoms only have bonds with the second layer and the other atoms in the first layer. This mean that these surface atoms have fewer bonds than the atoms in the bulk material, and therefore moves closer to the second layer to increase their bonding. As a result of this the second layer now experiences a higher density compared to the bulk, and to counteract this, they increase the distance to the third layer. This effect continues further into the

model as an oscillatory motion layer to layer. EAM not only gives an understanding of this phenomenon, but also gives a good forecast of the spacing between the different atomic layers. [11]

### 2.4.5 Visualization and analysis software

In this work the visualization software OVITO [19] has been used for illustrating the simulation results and give an understanding of them.

The centrosymmetry parameter (CSP) used in OVITO, is a measure of the irregularity of a lattice surrounding an atom which can be useful when investigating if the pattern around is perfect, containing a local defect or positioned at a surface. The CSP value  $p_{csp}$  is defined

$$p_{csp} = \sum_{i=1}^{N/2} |r_i + r_{i+N/2}|^2, \quad (2.22)$$

where  $r_i + r_{i+N/2}$  are two neighbor vectors from the central atom to a pair of opposite neighbor atoms. N is the number of nearest neighbors, in the case of bcc it is 8, for fcc it is 12. For a perfect lattice with no defects the CSP value will be zero, else it will be positive [20]. In OVITO it is often used with color coding which by a color scale makes it easy to get a good overview over the whole sample.

# 3 Simulations and results

In this section results from different simulations of tungsten samples will be presented. The result from the simulations performed in section 3.1-3.5 will be used in the later simulations containing defects. They will be used to choose suitable sample size, potential function, strain rate, boundary condition.

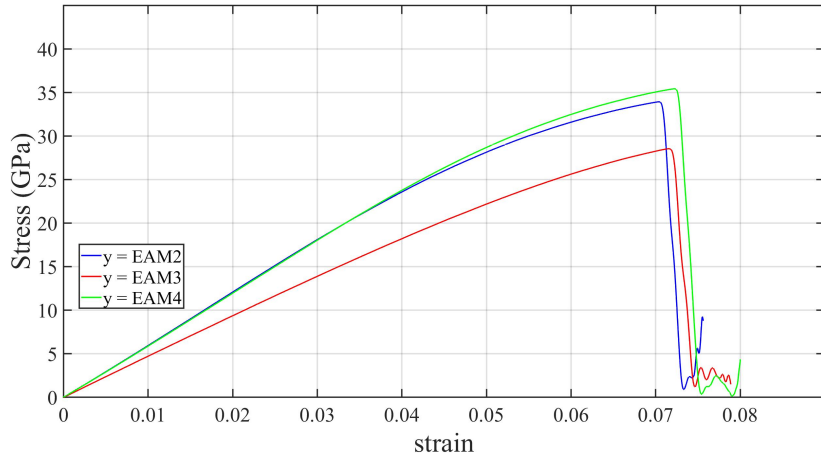
## 3.1 Potential dependence

Three different potential functions will be tested in this section: EAM2, EAM3 and EAM4. In [1] it is clear that the parameters of these potentials are completely different, among others the lattice parameter  $a_0$ . Simulations of samples with three different crystal orientations have been performed with EAM2, EAM3 and EAM4 separately, to find the most satisfactory potential for this work. The parameters used in these simulations are shown in Table 3.1 .

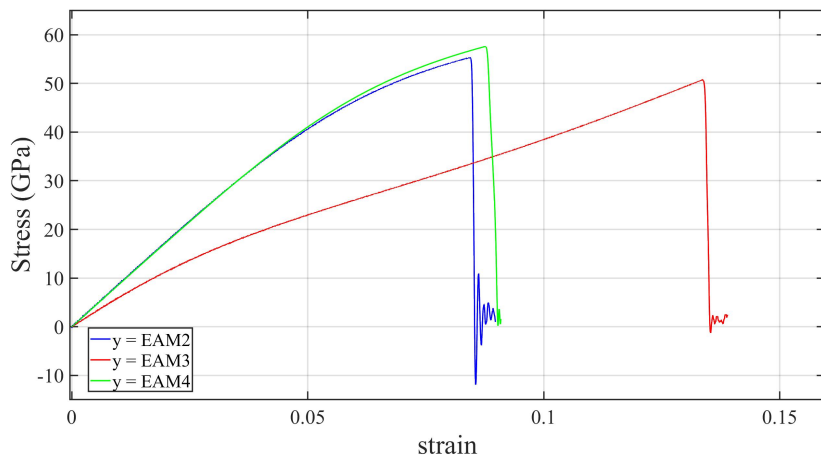
**Table 3.1:** Simulation parameters.

Relaxation steps	50000
Time step	5fs
Temperature	700K
Lattice parameter	3.140Å, 3.187Å and 3.143Å
Simulation box	100x24x24 unit cells
Crystal orientation	[1 0 0], [1 1 0] and [1 1 1]
Loading direction	[1 0 0].
Potential	EAM2, EAM3 and EAM4
Boundary conditions	pss
Statistical ensemble	NVT
Strain rate	$1 * 10^8/s$

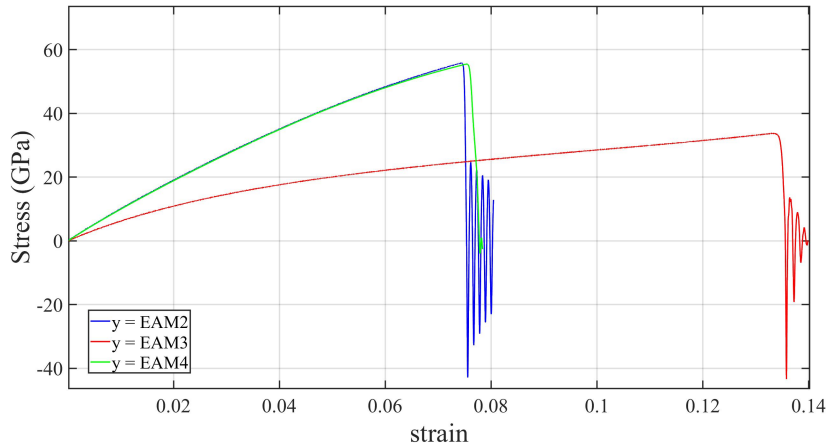
If one chooses to look at Young's modulus in the stress-strain curves in Figure 3.1 it is shown shows that Young's modulus will be about the same for EAM2 and EAM4 for the last two directions, for EAM3 it will be much lower in all directions. The strain at peak stress is almost the same for all three potentials in direction [1 0 0], but in direction [1 1 0] and [1 1 1] the strains for potential EAM3 are almost twice as large as for EAM2 and EAM4.



(a) Different potentials [1 0 0] direction



(b) Different potentials [1 1 0] direction



(c) Different potentials [1 1 1] direction

**Figure 3.1:** Stress-strain curves calculated using EAM2, EAM3 and EAM4 potentials for three crystal orientations, with simulation parameters according to Table 3.1 .

From looking at other stress-strain curves of tungsten at [1 1 1] direction in [21], it is clear that the EAM3 potential is not in agreement. In this reference, the [1 1 1] direction is the strongest, but in Figure 3.1(c) this is the weakest. Therefore the choice for this work will be either EAM2 or EAM4. Since these two are very similar

and EAM4 is the newest of them, EAM4 potential will be chosen for this work.

## 3.2 Strain rate dependence

Here the aim is to see if the stress-strain curves will look the same when changes are made in the strain rate. The parameters used in these simulations are shown in Table 3.2 .

**Table 3.2:** Simulation parameters.

Relaxation steps	50000
Time step	5fs
Temperature	700K
Lattice parameter	3.14Å
Simulation box	100x24x24 unit cells
Crystal orientation	[1 0 0]
Loading direction	[1 0 0]
Potential	EAM4
Boundary conditions	pss
Statistical ensemble	NVT
Strain rate	$1 * 10^5$ to $1 * 10^{10}/s$

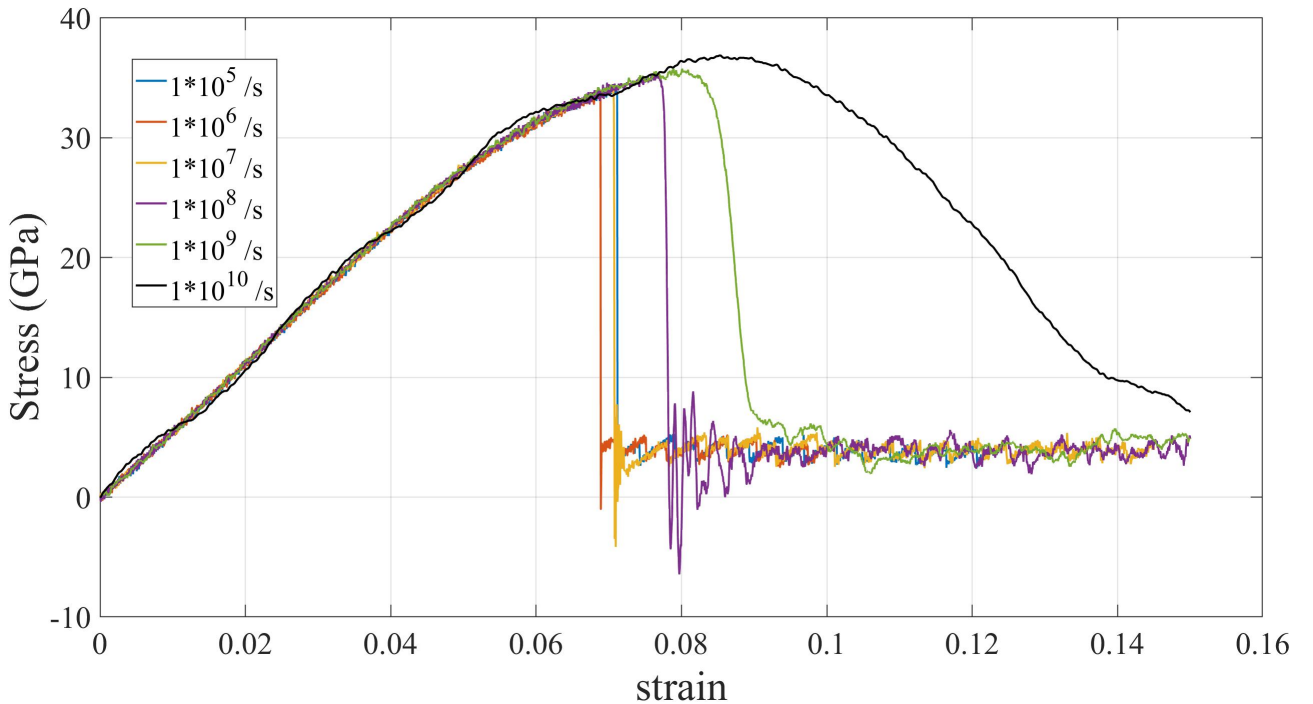


**Figure 3.2:** Stress-strain curves of different strain rates, simulation parameters according to Table 3.2 .

From the strain rate plot in Figure 3.2 it emerges that the speed of the deformation has no impact on Young's modulus, but when the strain rate exceeds  $1 * 10^8$  peak stress increases with the strain rate. In the two curves with the highest strain rates,

fracture don't seem to happen.

The dependence between the maximum stress and strain rate is primarily due to the dynamic wave effect that impedes the motion of dislocations. The rate-dependence of the maximum stress becomes weaker as the strain rate decreases. Thus, it exists a critical strain rate for single crystal metals, below which the material properties becomes less rate-insensitive. [22, p. 11]

When choosing strain rate, there are two important factors, time and accuracy. The lower the value of strain rate is, the more accurate the stress and strain values will be, but the simulation time will grow. In this work a strain rate of  $1 * 10^8$  will be used. The curves in Figure 3.2 shows much similarities with the curves in [22, p. 23].

### 3.3 Size effects and periodic- compared to non-periodic boundary condition.

As mentioned in section 2.1 , periodic boundary conditions best represent bulk material in a simulation. In this section stress-strain curves of non-periodic simulations with different simulation box sizes will be plotted against a curve from a periodic simulation. The goal is to see if a sample with non-periodic boundary conditions can represent bulk material in a good way. If this is the case, the next step will be to examine which simulation box size it takes to do this in a satisfactory manner. For this simulation the parameters can be seen in Table 3.3 .

**Table 3.3:** Simulation parameters.

Relaxation steps	50000
Time step	5fs
Temperature	700K
Lattice parameter	3.14Å
Simulation box	100x12x12, 100x24x24, 100x36x36, 100x48x48 and 100x60x60 unit cells
Crystal orientation	[1 0 0]
Loading direction	[1 0 0]
Potential	EAM4
Boundary conditions	pss and ppp
Statistical ensemble	NVT and NPT
Strain rate	$1 * 10^8/s$

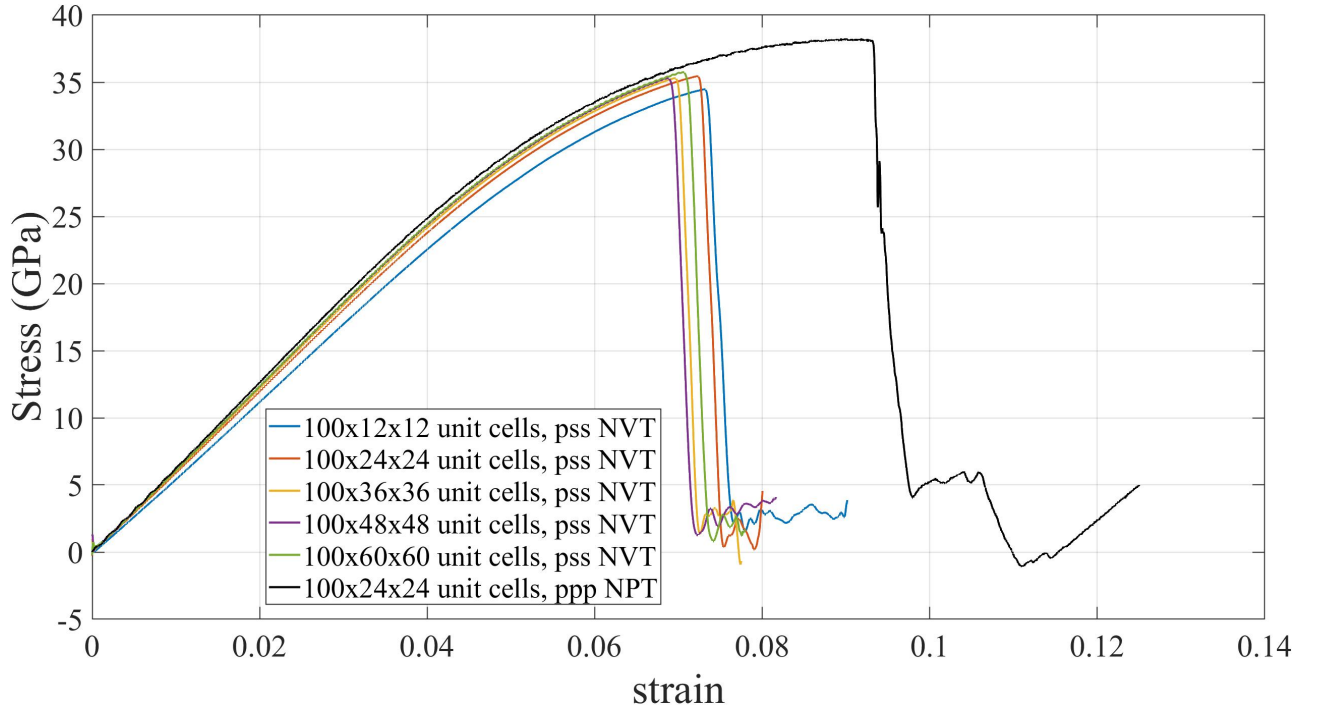


**Figure 3.3:** Stress-strain curves of periodic- compared to non-periodic boundary conditions with varying simulation box sizes, simulation parameters according to Table 3.3 .

Figure 3.3 shows that the samples with non-periodic boundary conditions do not represent bulk material well, with respect to peak stress and fracture strain, regardless simulation box size. The smaller the sample, the larger the strain at peak stress, with the exception of 100x60x60. This can depend on the fact that larger specimens offer more spaces for dislocation to happen. Similarities can be seen in [22, p. 21] . It clearly can be seen that for a smaller sample, 100x12x12 unit cells, there exist a difference in Young's modulus, but the larger the simulation box size becomes, the closer one get to the Young's modulus of the periodic sample.

For the non-periodic simulations done in this work a sample size of 100x24x24 unit cells is chosen, which is relatively close to Young's modulus for bulk material properties, and is requires less propagation time compared to the sample size of 100x60x60 unit cells.

### 3.4 Temperature dependence

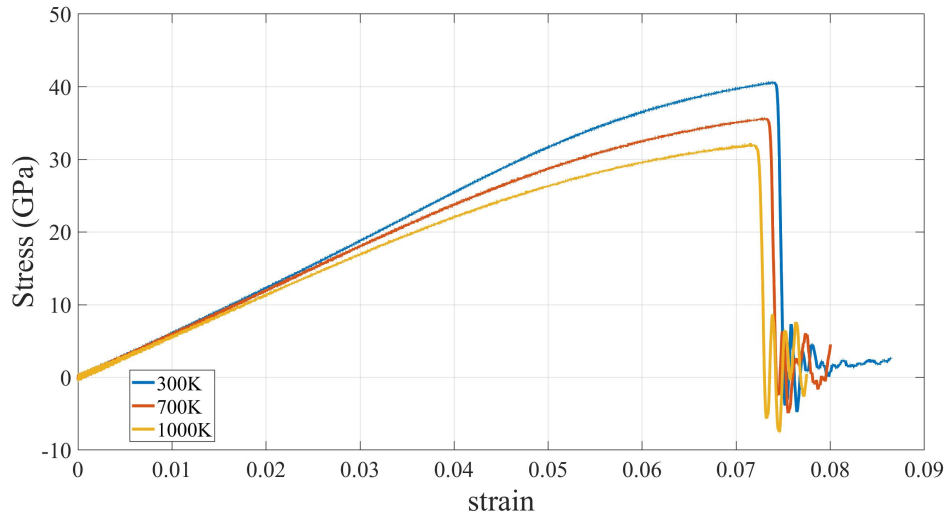
Now consider the influence temperature has on the material properties. Three different directions,  $[1\ 0\ 0]$ ,  $[1\ 1\ 0]$  and  $[1\ 1\ 1]$  will here be taken into consideration. For this simulation the parameters can be seen in Table 3.4 .

**Table 3.4:** Simulation parameters.

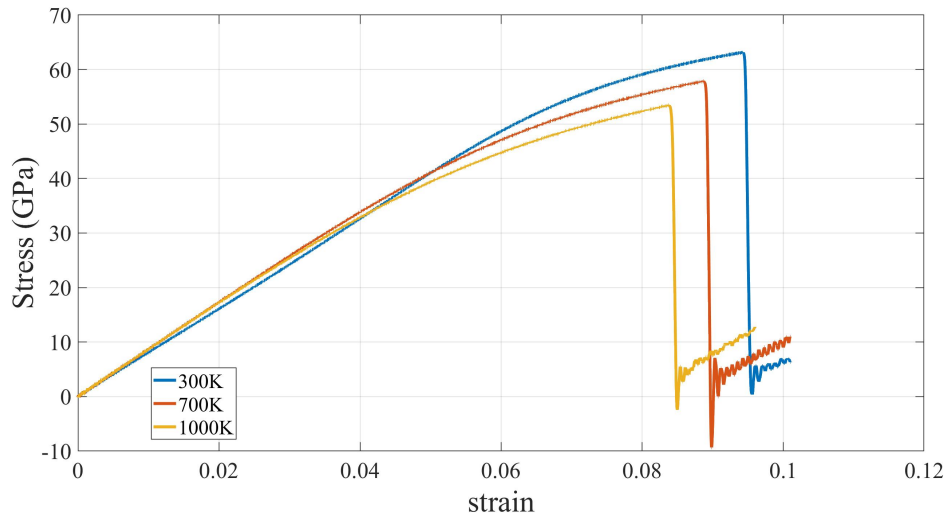
Relaxation steps	50000
Time step	5fs
Temperature	300K, 700K and 1000K
Lattice parameter	3.14Å
Simulation box	100x24x24 unit cells
Crystal orientation	[1 0 0], [1 1 0] and [1 1 1]
Loading direction	[1 0 0]
Potential	EAM4
Boundary conditions	pss
Statistical ensemble	NVT
Strain rate	$1 * 10^8/s$

Figure 3.4 shows that for directions [1 0 0] and [1 1 0], a relatively large difference in maximum stresses for the different temperatures can be seen, while for [1 1 1] the difference is not that large. It is found that Young's modulus for the first two directions is affected by the temperature, while in the third case it remains almost the same for all temperatures. This is something that agrees with the result in [21, p. 17732]. For the [1 0 0] direction the differences between the strains at peak stresses are small, while there are larger differences in the two other directions.

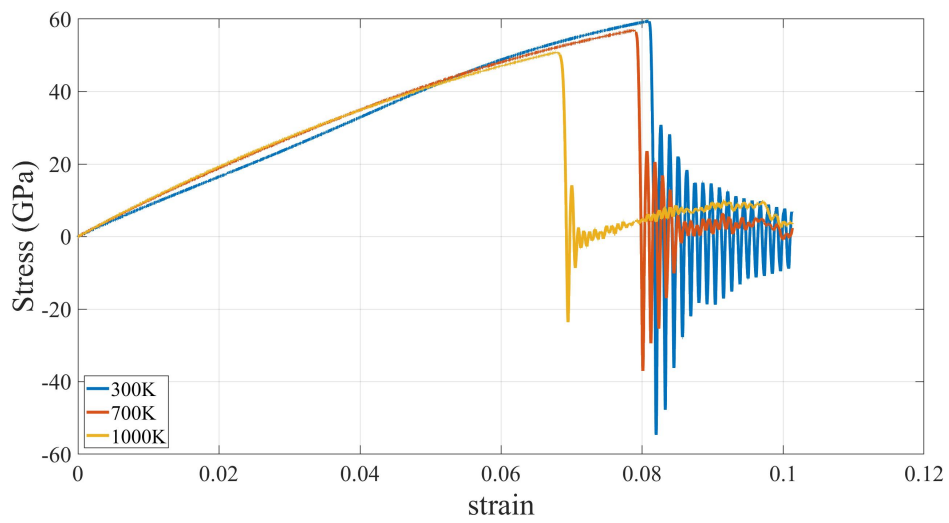




(a) Crystal orientation [1 0 0].



(b) Crystal orientation [1 1 0].



(c) Crystal orientation [1 1 1].

**Figure 3.4:** Stress-strain curves over the influence of temperature, simulation parameters according to Table 3.4 .

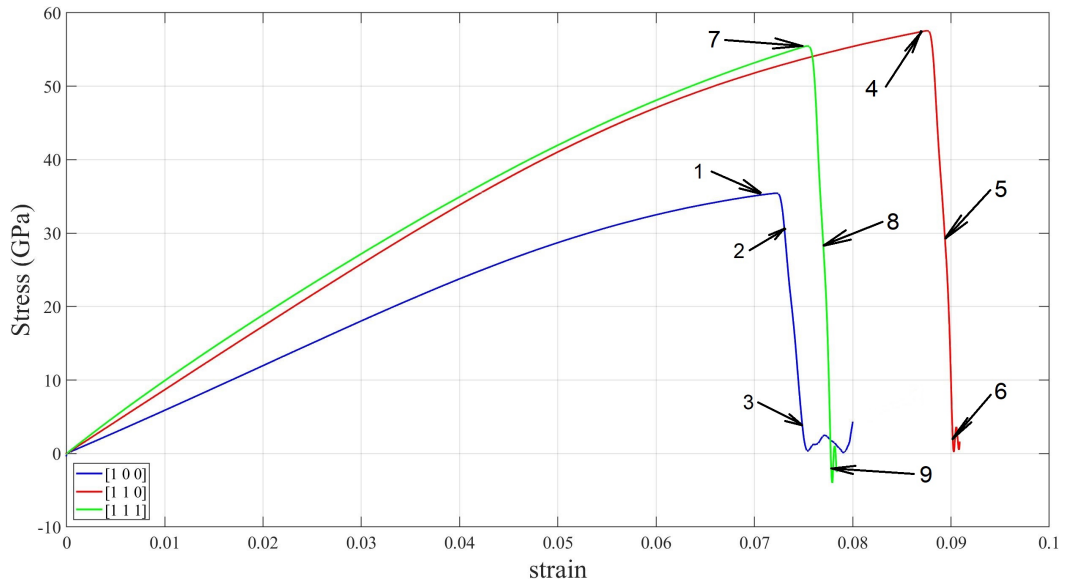
### 3.5 Influence of crystal orientation

In this section the material properties of both a nanowire as well as bulk material will be simulated for three different crystal orientations. Boundary conditions pss and statistical ensemble NVT will correspond to the nanowire, while ppp and NPT is used to represent bulk atoms. The parameters used in these simulations are shown in Table 3.5 .

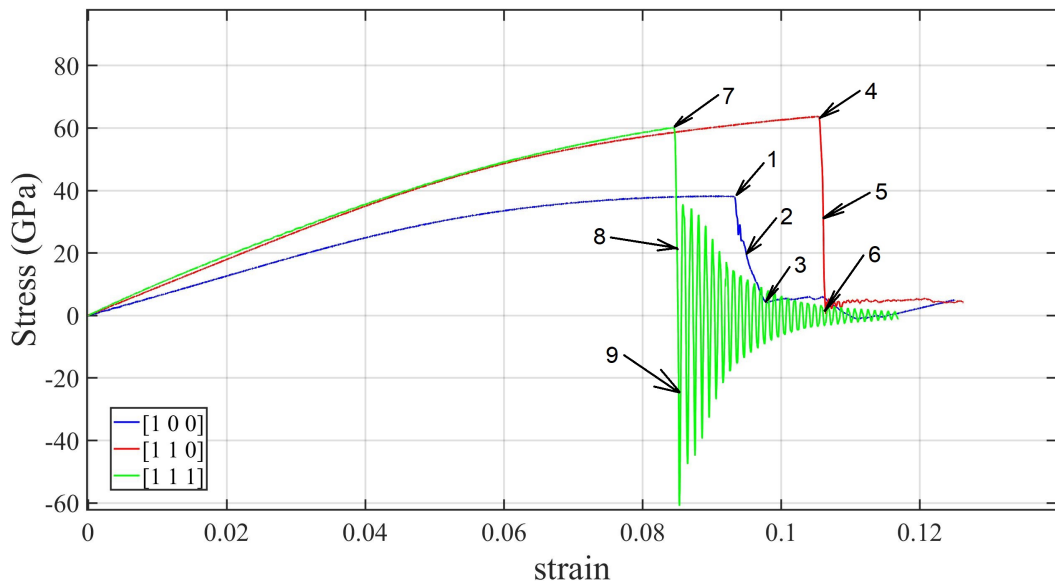
**Table 3.5:** Simulation parameters.

Relaxation steps	50000
Time step	5fs
Temperature	700K
Lattice parameter	3.14Å
Simulation box	100x24x24 unit cells
Crystal orientation	[1 0 0], [1 1 0] and [1 1 1]
Loading direction	[1 0 0]
Potential	EAM4
Boundary conditions	pss and ppp
Statistical ensemble	NVT and NPT
Strain rate	$1 * 10^8/s$

Figure 3.5 shows stress-strain curves for three crystal orientations, with nanowire-respectively bulk material properties.



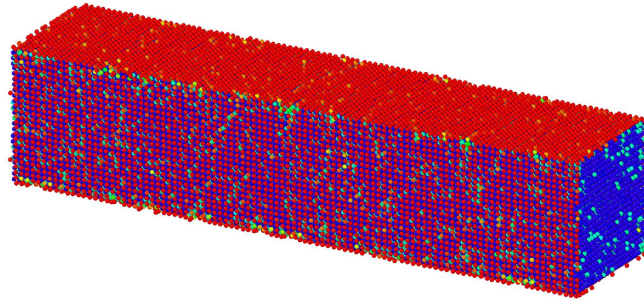
(a) Stress-strain curves for boundary conditions pss, with statistical ensemble NVT propagation. CSP images of 1-3 can be seen in Figure 3.6. CSP images of 4-6 can be seen in Figure 3.7. CSP images of 7-9 can be seen in Figure 3.8.



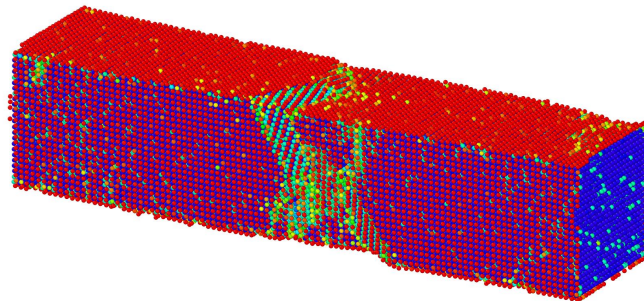
(b) Stress-strain curves for boundary conditions ppp, with statistical ensemble NPT propagation. CSP images of 1-3 can be seen in Figure 3.9. CSP images of 4-6 can be seen in Figure 3.10. CSP images of 7-9 can be seen in Figure 3.11.

**Figure 3.5:** Different crystal orientations, simulation parameters according to Table 3.5 .

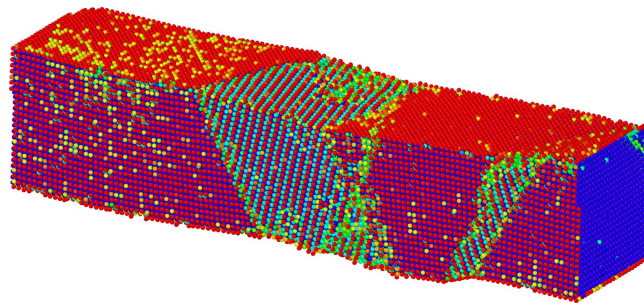
Figures 3.6 to 3.11 shows the microstructure of the samples during the simulation, of the positions specified in Figure 3.5.



(a) Position 1 in Figure 3.5a, strain 0.07275 .



(b) Position 2 in Figure 3.5a, strain 0.07375 .



(c) Position 3 in Figure 3.5a, strain 0.07425 .

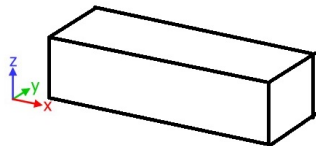
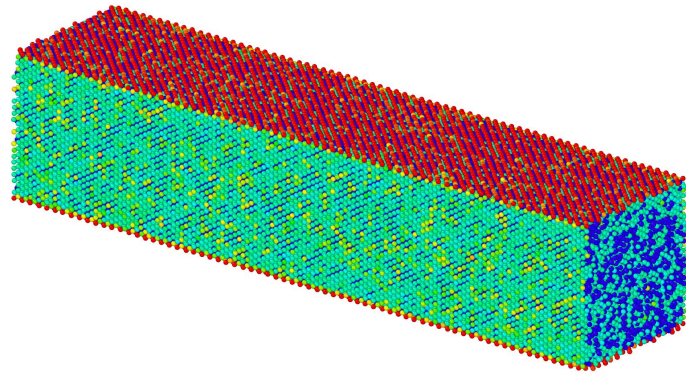
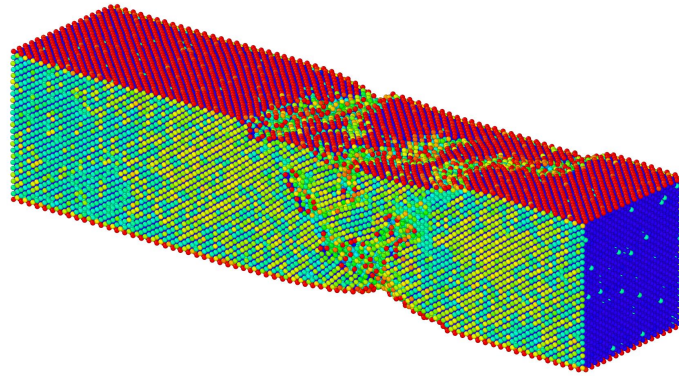


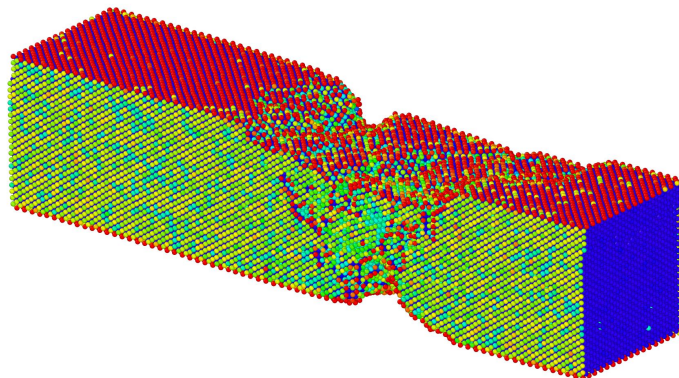
**Figure 3.6:** Orientation  $[1\ 0\ 0]$  from Figure 3.5a



(a) Position 4 in Figure 3.5a, strain 0.0875 .



(b) Position 5 in Figure 3.5a, strain 0.08965 .



(c) Position 6 in Figure 3.5a, strain 0.09026 .

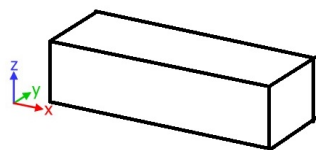
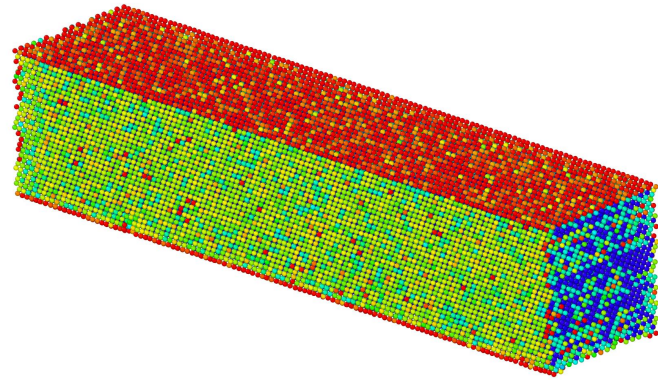
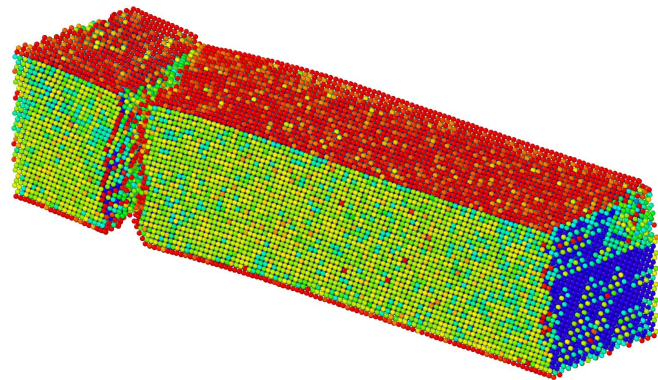


**Figure 3.7:** Orientation  $[1\ 1\ 0]$  from Figure 3.5a

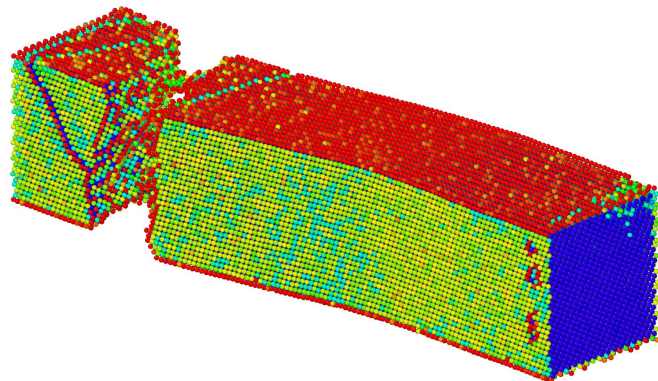




(a) Position 7 in Figure 3.5a, strain 0.07522 .



(b) Position 8 in Figure 3.5a, strain 0.07699 .



(c) Position 9 in Figure 3.5a, strain 0.07775 .

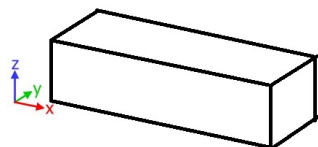
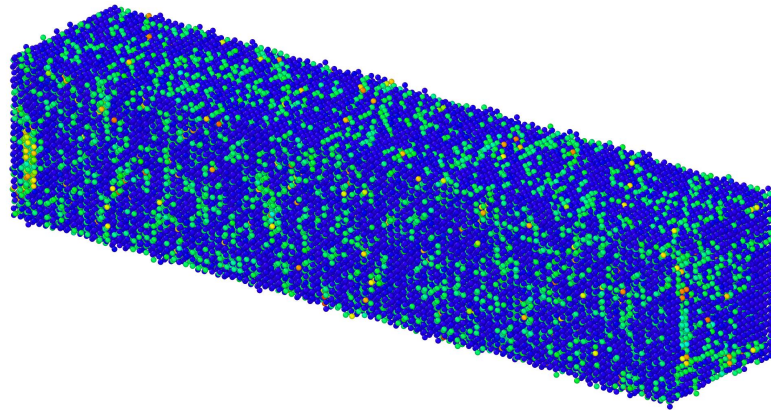
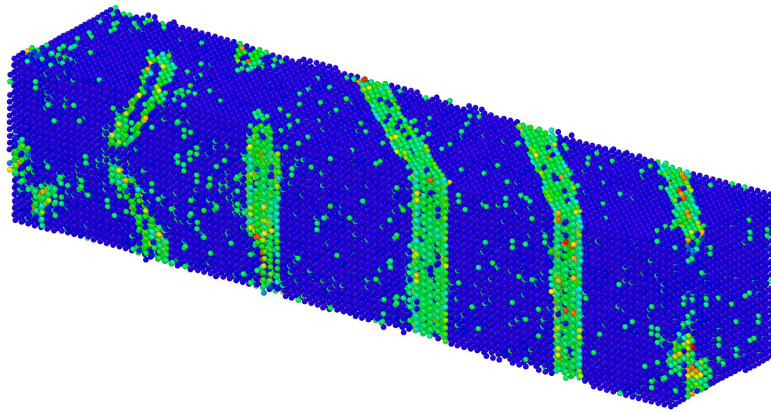


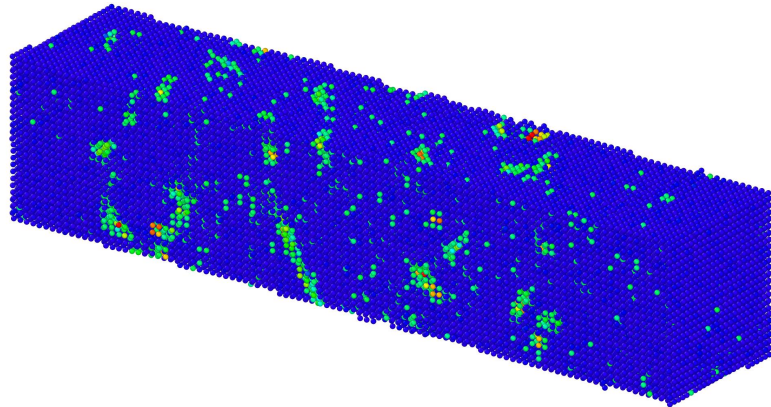
**Figure 3.8:** Orientation [1 1 1] from Figure 3.5a



(a) Position 1 in Figure 3.5b, strain 0.09318 .



(b) Position 2 in Figure 3.5b, strain 0.09545 .



(c) Position 3 in Figure 3.5b, strain 0.09763 .

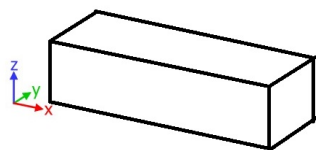
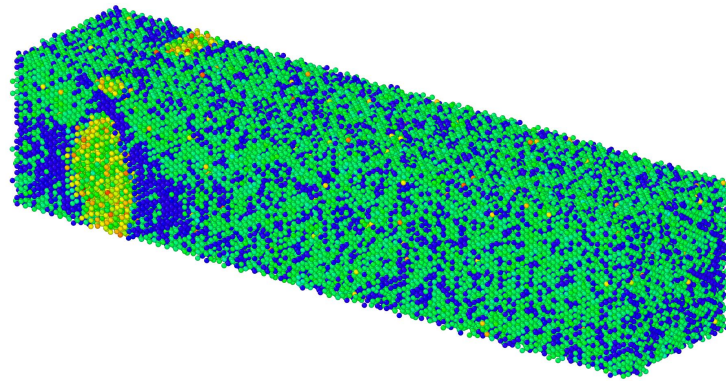
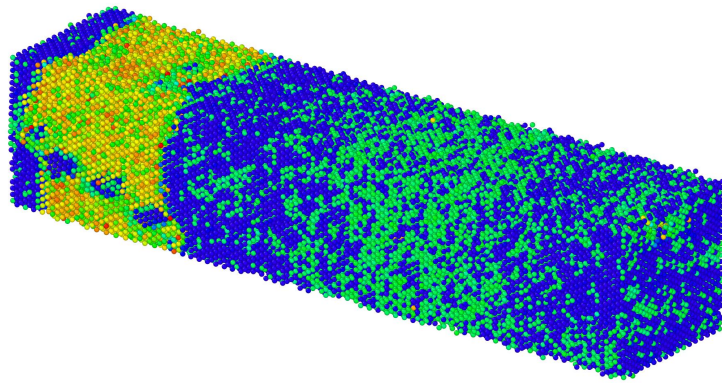


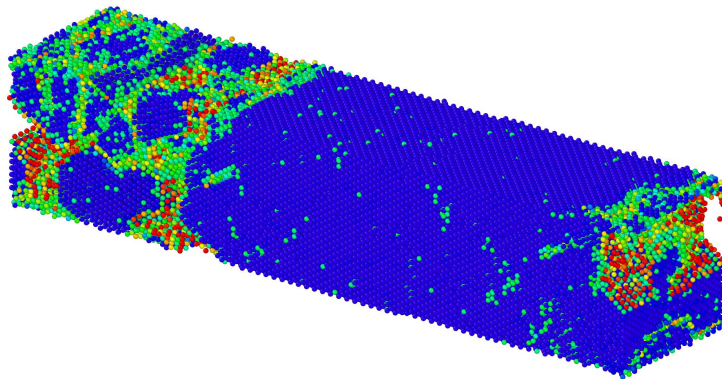
**Figure 3.9:** Orientation  $[1\ 0\ 0]$  from Figure 3.5b



(a) Position 4 in Figure 3.5b, strain 0.1054 .



(b) Position 5 in Figure 3.5b, strain 0.1059 .



(c) Position 6 in Figure 3.5b, strain 0.1064 .

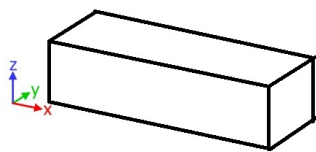
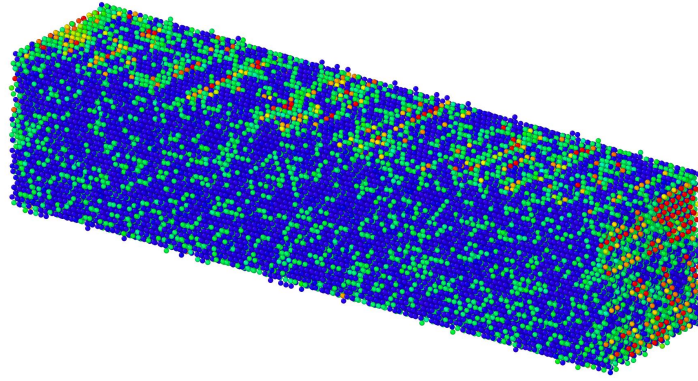
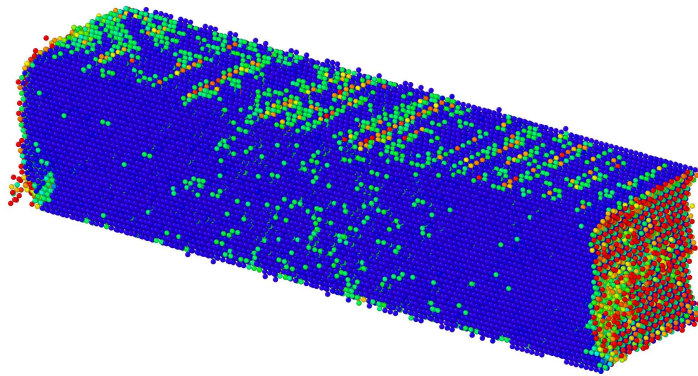


**Figure 3.10:** Orientation  $[1\ 1\ 0]$  from Figure 3.5b .

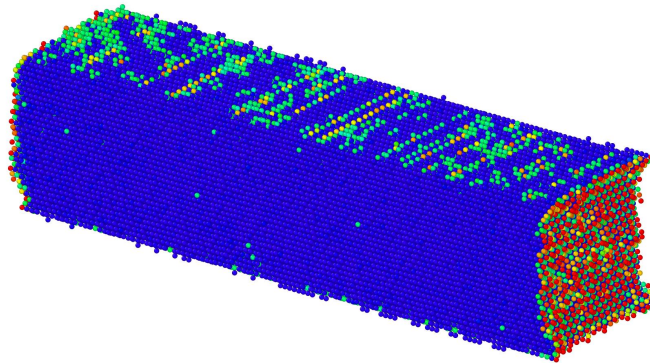




(a) Position 7 in Figure 3.5b, strain 0.08446 .



(b) Position 8 in Figure 3.5b, strain 0.08488 .



(c) Position 9 in Figure 3.5b, strain 0.0853 .

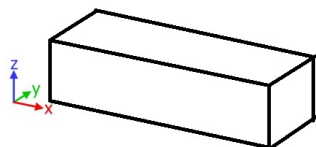


**Figure 3.11:** Orientation  $[1\ 1\ 1]$  from Figure 3.5b

For the  $[1\ 0\ 0]$  orientations seen in Figure 3.6, slipping of local atomic layers happens in  $\{2\ 1\ 1\}$  plane, and for Figure 3.9, slipping of local atomic layers happens in  $\{1\ 1$

0} plane. For the [1 1 0] orientations seen in Figures 3.7 and 3.10, slipping of local atomic layers happens in {2 1 1} plane in the first case, and in the second case no slipping happened. For the [1 1 1] orientations seen in Figure 3.8 and 3.11 no slipping were observed, just clean breaks.

When looking at Figures 3.6 to 3.11 one can clearly see the differences between boundary conditions pss and ppp.

Necking do not exist for ppp, while a small hint of this, is happening right before the fracture for all three pss simulations.

Figure 3.5 shows that [1 0 0] direction is the weakest for both curves, and [1 1 0] is the strongest.

If one look at Young's modulus at [1 1 0] and [1 1 1] directions has almost the same Young's modulus, while for [1 0 0] direction, this much lower.

The elastic stage starts at zero strain and ends where the stress has reached its maximum value. For pss this is about 7.3% for [1 0 0], 8.8% for [1 1 0] and 7.5% for [1 1 1]. For ppp the plastic stage starts at strains about 9.3% for [1 0 0], 10.5% for [1 1 0] and 8.4% for [1 1 1]. The plastic stage starts when the elastic stage ends.

The differences between pss and ppp regarding Young's modulus are small, but pss is lower. The reason why the plastic stage starts earlier in pss is that here a surface exists compared to in ppp, where only bulk atoms exist. The weaker bonding of the surface atoms causes necking, this finally leads to fracture.

## 3.6 Defect sensitivity

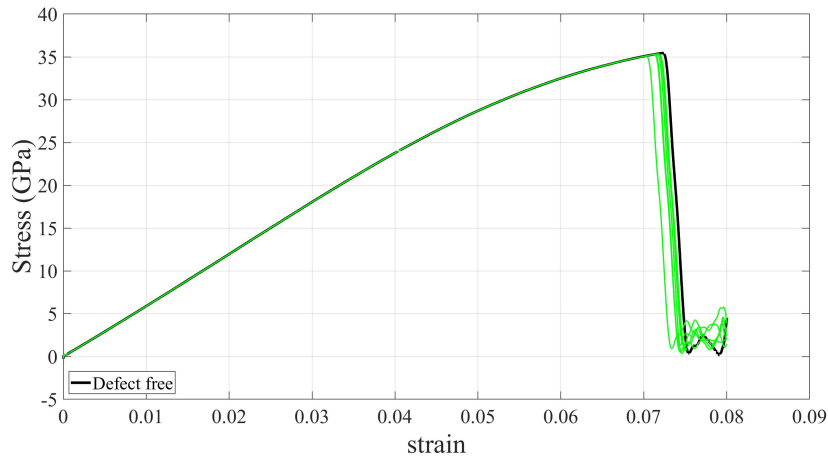
### 3.6.1 Vacancies

For this work vacancy densities between  $1 * 10^{23}$  and  $1 * 10^{25}$  per  $m^3$  are relevant. Since one  $m^3$  holds about  $6.44 * 10^{28}$  tungsten atoms, this defects corresponds to values between  $1.55 * 10^{-4}\%$  and  $1.55 * 10^{-2}\%$ . But because  $1.55 * 10^{-4}\%$ , in a sample of size 100x24x24 unit cells, only corresponds to 0.19 atoms, this number will be excluded. Instead the defect values tested will lie between  $1.55 * 10^{-3}\%$  and  $1.55 * 10^{-1}\%$ . The vacancy positions will be randomly distributed inside the tungsten sample, so several simulations with each model will be tested in order to find out if the placements of the vacancies have any impact on the results. The parameters used in these simulations are shown in Table 3.6 .

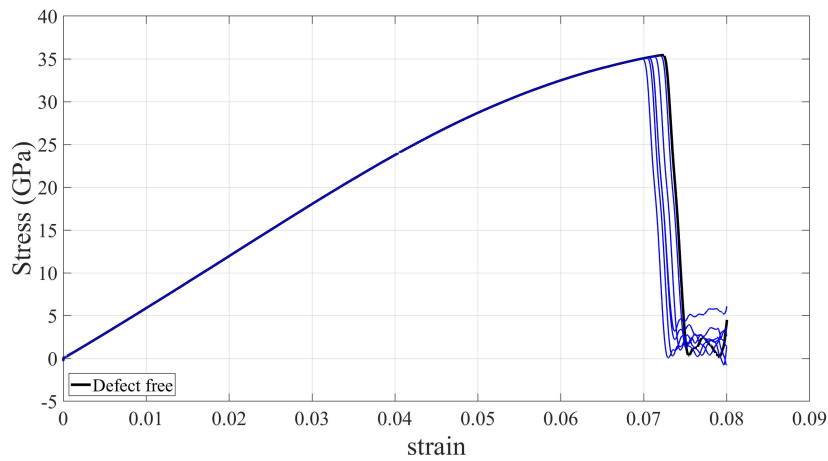
**Table 3.6:** Simulation parameters.

Relaxation steps	50000
Time step	5fs
Temperature	700K
Lattice parameter	3.14Å
Simulation box	100x24x24 unit cells
Crystal orientation	[1 0 0], [1 1 0] and [1 1 1]
Loading direction	[1 0 0]
Potential	EAM4
Boundary conditions	pss
Statistical ensemble	NVT
Strain rate	$1 * 10^8 / s$
Vacancy density	between $1 * 10^{24}$ and $1 * 10^{26} / m^3$

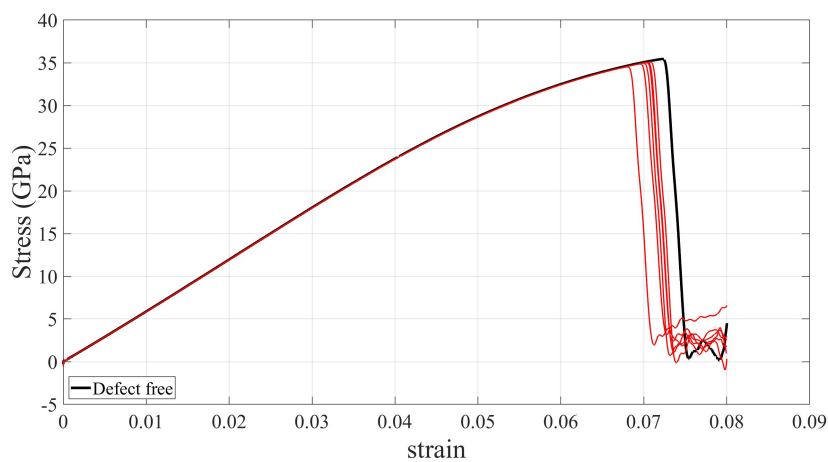
Firstly it was confirmed that the vacancies which were placed randomly in the material before the relaxation process, remained when this process was finished. This was controlled in the program OVITO, by finding the positions before and after the relaxation process, and was proven right for vacancies positioned within the bulk atoms. At the surface some cases were found where the vacancy site was moved, but not more than one atomic site. The positions of the vacancies when the relaxation was finished remained constant until the plastic stage started. As can be seen from Figure 3.12 and 3.14, the introduction of vacancies between  $1.55 * 10^{-3}\%$  and  $1.55 * 10^{-1}\%$  do not seem to have any significantly change in Young's modulus, but it seems that a small difference occurs in the strain at peak stress. This shows that the positions of the randomly placed vacancies are important with respect to material properties. For orientation [1 0 0] a comparison between the most disadvantageous, and the most favorable position of vacancies are put together in Figure 3.13, and Table 3.7 is based on these positions. In this table it can be seen that it is not just the number of surface vacancies that influences when the sample will break. For example in vacancy density  $1 * 10^{26}$  the sample that breaks first (the most disadvantageous sample), has 12 surface vacancies, while the the most favorable sample has 14 surface vacancies. If one studies the distribution of these, the most disadvantageous sample has 9 out of 12 surface vacancies on one of the four sides, while the most favorable sample has a more even distribution over its sides. This shows that if the vacancies are grouped or gathered on the same surface, this affects the material properties in a negative way. Therefore the simulation in the following section will be to see which impact vacancy clusters have on the properties of tungsten.



(a) The green curves corresponds to six randomly positioned vacancies with vacancy density  $1 * 10^{24} \text{vacancies}/m^3$ .

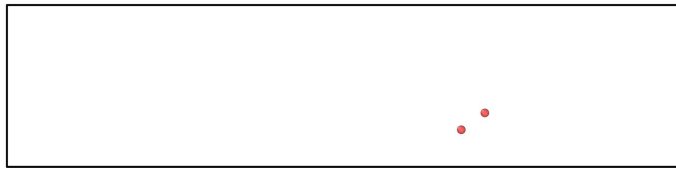


(b) The blue curves corresponds to six randomly positioned vacancies with vacancy density  $1 * 10^{25} \text{vacancies}/m^3$ .



(c) The red curves corresponds to six randomly positioned vacancies with vacancy density  $1 * 10^{26} \text{vacancies}/m^3$ .

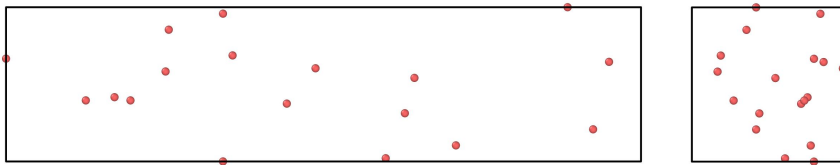
**Figure 3.12:** Stress-strain curves for randomly positioned vacancies, lattice orientation  $[1 0 0]$ . Simulation parameters according to Table 3.6 .



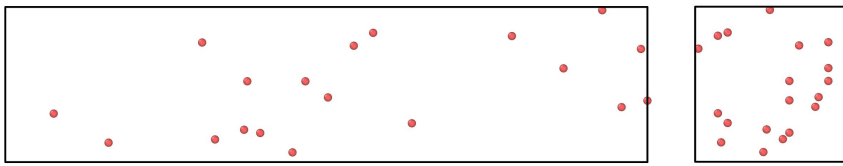
(a) Most disadvantageous positions of  $1 * 10^{24} \text{vacancies}/m^3$ .



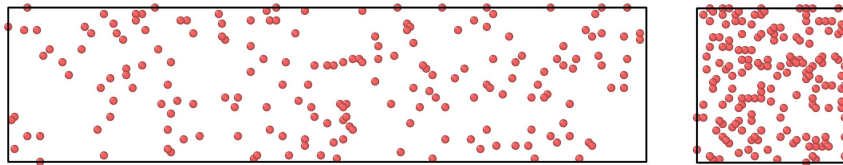
(b) Most favorable positions of  $1 * 10^{24} \text{vacancies}/m^3$ .



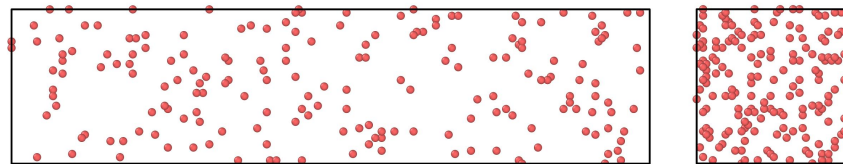
(c) Most disadvantageous positions of  $1 * 10^{25} \text{vacancies}/m^3$ .



(d) Most favorable positions of  $1 * 10^{25} \text{vacancies}/m^3$ .



(e) Most disadvantageous positions of  $1 * 10^{26} \text{vacancies}/m^3$ .



(f) Most favorable positions of  $1 * 10^{26} \text{vacancies}/m^3$ .

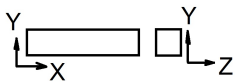
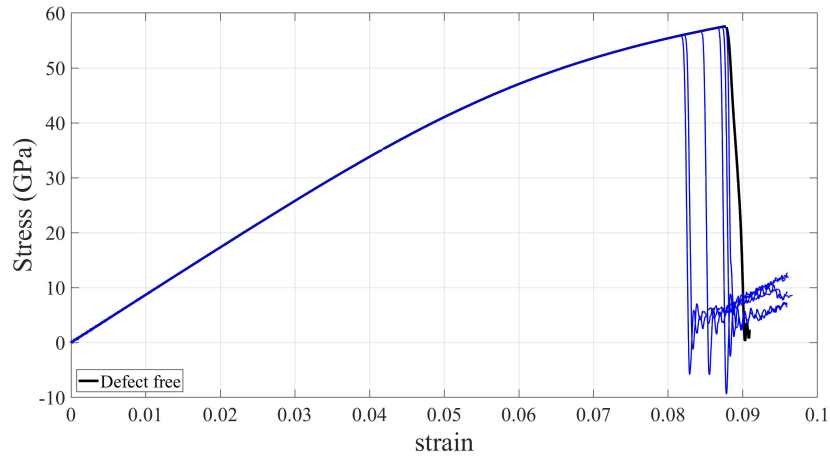


**Figure 3.13:** Comparison between the most disadvantageous and most favorable vacancy positions for the curves in Figure 3.12, with respect to material properties, for crystal orientation  $[1\ 0\ 0]$ . The red dots represent vacancies.

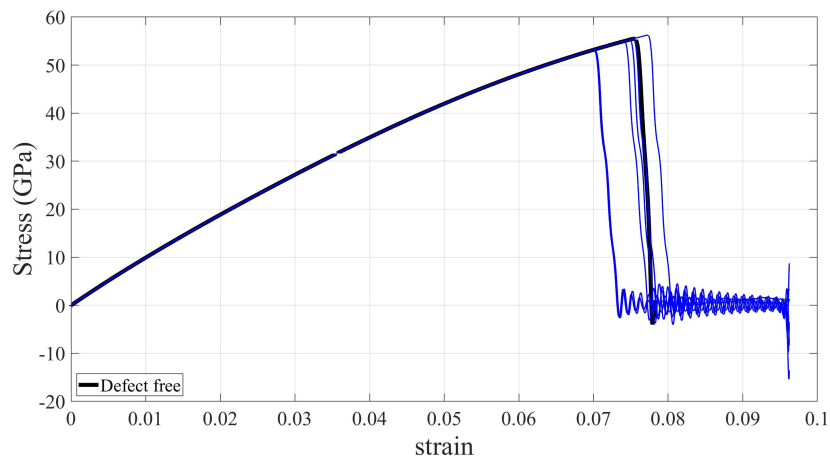
**Table 3.7:** Influence of vacancies on material properties, for crystal orientation [1 0 0].  
This table is based on the positions shown in Figure 3.13.

Vacancy density	Total number of vacancies	Most disadvantageous case, number of surface vacancies, distribution over its 4 non-periodic sides.	Most favorable case, number of surface vacancies, distribution over its 4 non-periodic sides.
$1 \times 10^{24}$	2	0 0,0,0,0	0 0,0,0,0
$1 \times 10^{25}$	19	2 1,0,1,0	0 0,0,0,0
$1 \times 10^{26}$	187	12 9,2,1,0	14 6,3,2,3

In Figure 3.14 stress-strain curves are shown for a vacancy density of  $1 \times 10^{25} \text{vacancies}/m^3$  and a crystal orientation [1 1 0] and [1 1 1]. The spread of the curves is larger here compared to in lattice orientation [1 0 0]. An explanation to this is that crystals with these orientations contain fewer unit cells in comparison to orientation [1 0 0]. Because of this the size of the vacancy fraction will be larger than compared to orientation [1 0 0]. Vacancies here have a greater impact on the material properties.



(a) Lattice orientation [1 1 0]



(b) Lattice orientation [1 1 1]

**Figure 3.14:** Stress-strain curves for randomly positioned vacancies. The blue curves corresponds to six randomly positioned vacancies with vacancy density  $1 * 10^{25} \text{vacancies}/\text{m}^3$ , lattice orientation [1 1 0] and [1 1 1], simulation parameters according to Table 3.6 .

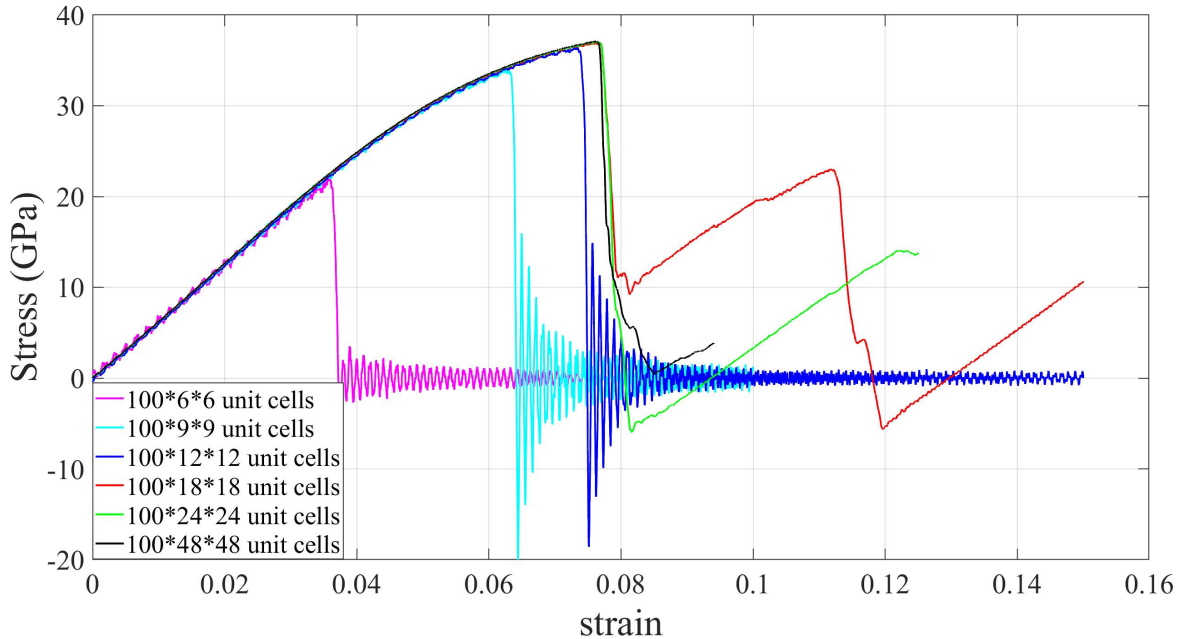
### 3.6.2 Vacancy clusters

In this simulation one will study the influence of several missing atoms close together in the middle of bulk material will have on the material properties. Using periodic boundary conditions, effects from the surface will not affect the result. The parameters used in these simulations are shown in Table 3.8

**Table 3.8:** Simulation parameters.

Relaxation steps	50000
Time step	5fs
Temperature	700K
Lattice parameter	3.14Å
Simulation box	100x24x24 unit cells
Crystal orientation	[1 0 0]
Loading direction	[1 0 0]
Potential	EAM4
Boundary conditions	ppp
Statistical ensemble	NPT
Strain rate	$1 * 10^8/s$
Number of vacancies	1, 2, 4,..., 128

As a first step it will be confirmed if the sample size has any impact on the obtained material properties. The spheres of missing atoms could, if the size of these are large in comparison to the samples, interact since these simulations are performed with periodic boundary conditions. This test will be done with the largest number of vacancies, i.e 128.

**Figure 3.15:** Stress-strain curves of six different sample sizes containing a vacancy cluster with size 128, simulation parameters according to Table 3.8 .

As can be seen in Figure 3.15 , the smallest sample sizes of 100x6x6, 100x9x9 and 100x12x12 unit cells are clearly affected by the vacancy cluster of size 128, their curves differing from the other three closely gathered curves. Thus for this simulation a sample size of 100x24x24 unit cells is chosen.



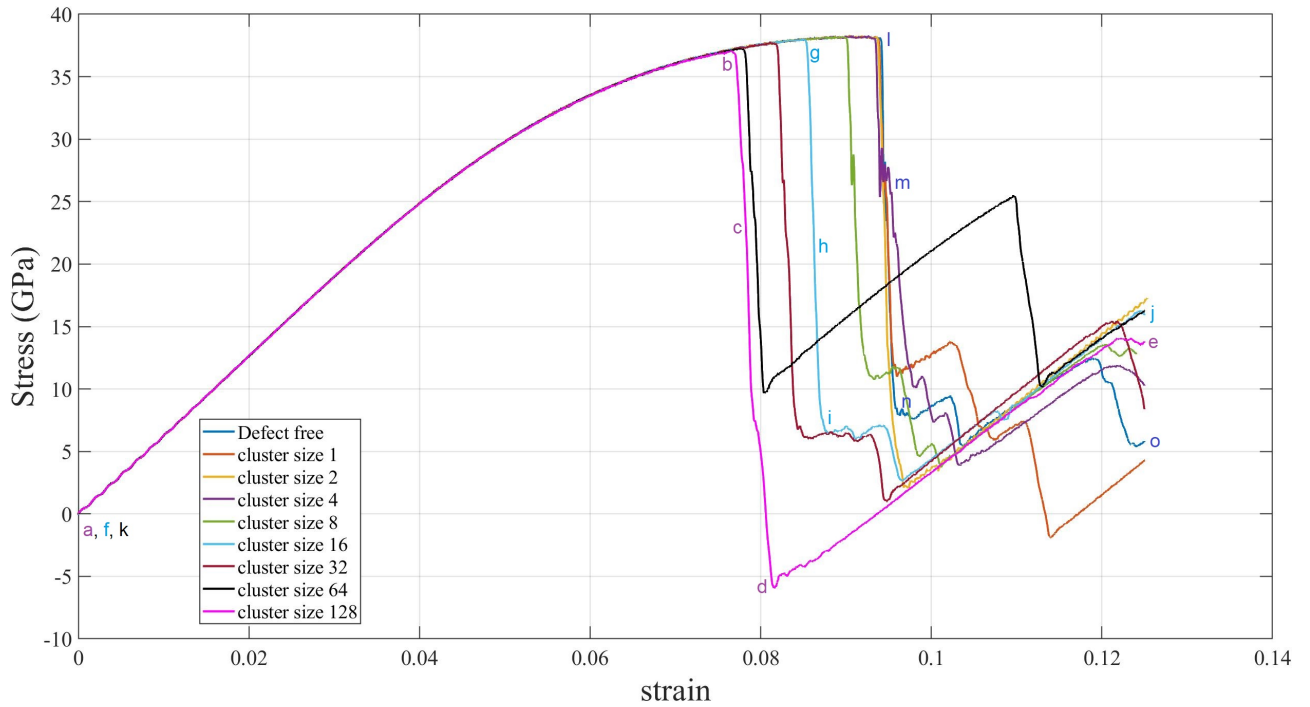
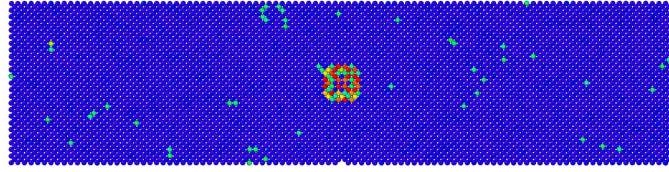


**Figure 3.16:** Stress-strain curves of samples containing vacancy clusters of different sizes, simulation parameters according to Table 3.8 .

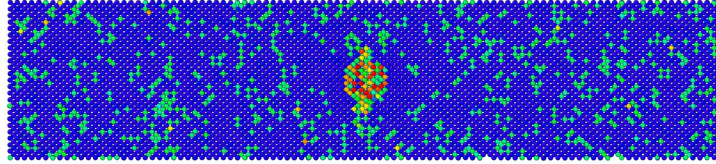
As can be seen from Figure 3.16, the occurrence of vacancy clusters results in both reduced peak stresses and the strains at peak stresses. This can clearly be seen when the vacancy cluster sizes are around 8 vacancies and upwards. The larger the vacancy cluster, the lower the strain at peak stress. However, the different sizes of the cavities don't seem to have any impact on Young's modulus.

From the images of the samples containing vacancy clusters, Figure 3.17 and 3.18 , it can be seen that the plastic deformation starts at the position of the vacancy clusters. Already in the first sub-picture a), where the tensile test starts, the color code of CSP values reveals that the neighbouring atoms of the vacancy clusters are treated as surface atoms. The second sub-pictures b), shows the samples at their peak stresses. Here it is revealed that the plastic deformation starts at the atoms surrounding the hole. Thereafter deformation happens, see sub-pictures c), where it is shown that there exists a difference in deformation procedure between vacancy cluster size 128 and 16. The larger the vacancy cluster, the larger the risk of interaction between them. For vacancy cluster size 128 the deformation starts in the direction of the shortest distance from one vacancy cluster to another, since it is periodic in all directions. For vacancy cluster size 16 the deformation starts in one of the possible slip planes for tungsten. Figure 3.19 of the defect free sample shows a completely different deformation process, which happens at a higher strain value.

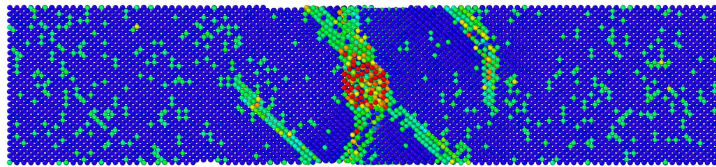
Thus the cluster works as a seed for plastic deformations, the larger the cluster, the earlier the deformation happens.



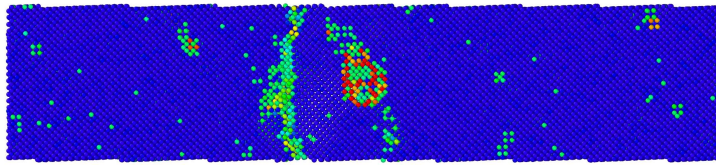
(a) Position a in Figure 3.16, strain 0.



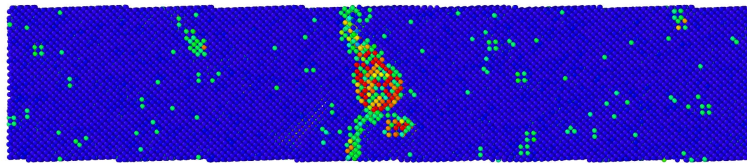
(b) Position b in Figure 3.16, strain 0.07652.



(c) Position c in Figure 3.16, strain 0.07865.



(d) Position d in Figure 3.16, strain 0.0813.



(e) Position e in Figure 3.16, strain 0.125.

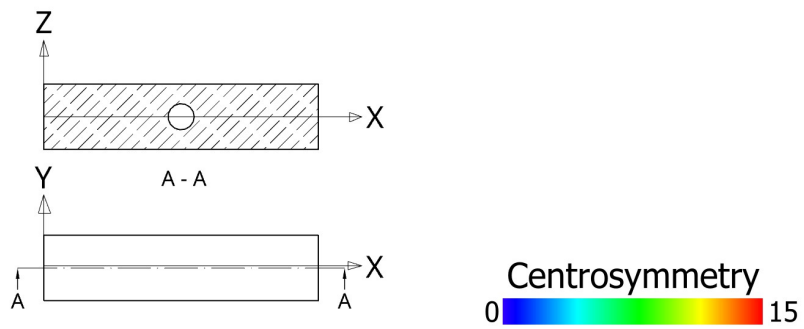
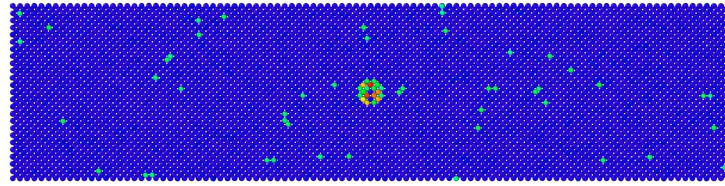
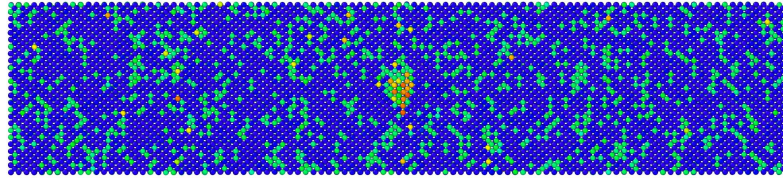


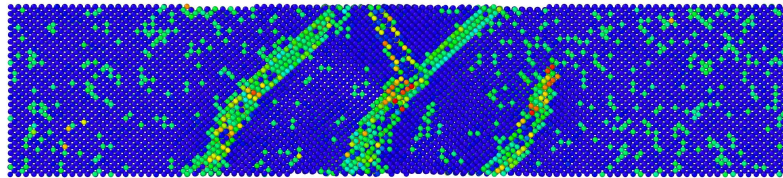
**Figure 3.17:** Deformation of cluster size 128 in Figure 3.16, seen in cross section A-A with  $0 \leq CSP \leq 15$ .



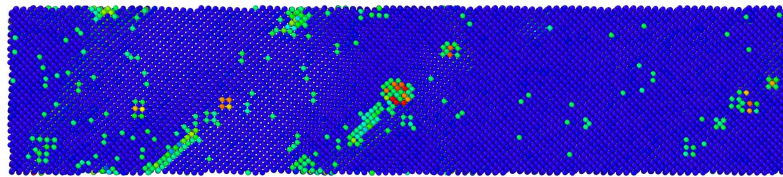
(a) Position f in Figure 3.16, strain 0.



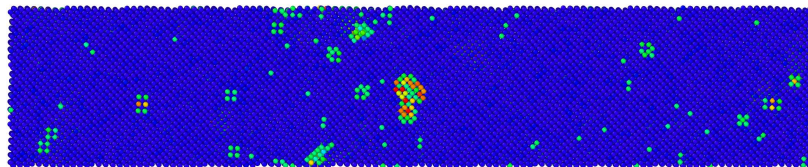
(b) Position g in Figure 3.16, strain 0.08515.



(c) Position h in Figure 3.16, strain 0.0862.



(d) Position i in Figure 3.16, strain 0.0876.



(e) Position j in Figure 3.16, strain 0.125.

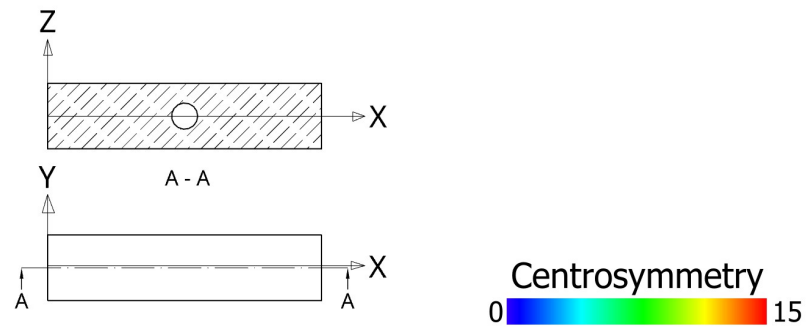
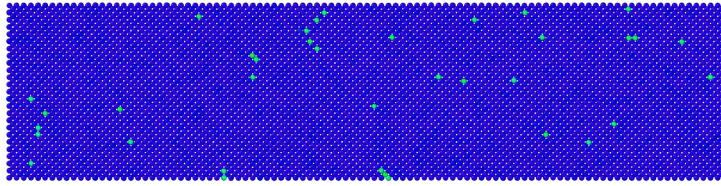
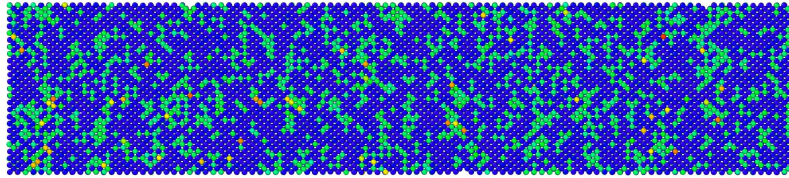


**Figure 3.18:** Deformation of cluster size 16 in Figure 3.16, seen in cross section A-A with  $0 \leq CSP \leq 15$ .

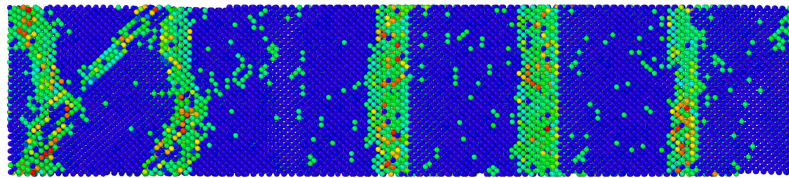




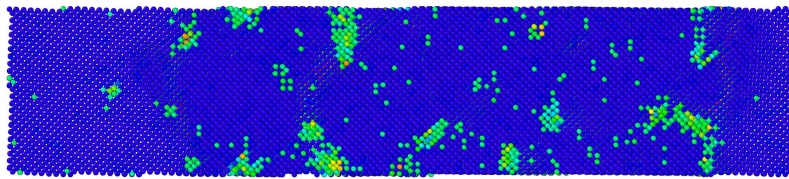
(a) Position k in Figure 3.16, strain 0.



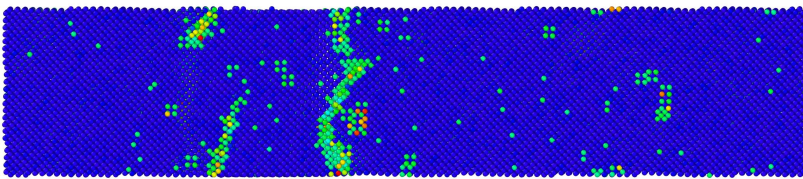
(b) Position l in Figure 3.16, strain 0.094.



(c) Position m in Figure 3.16, strain 0.0945.



(d) Position n in Figure 3.16, strain 0.09583.



(e) Position o in Figure 3.16, strain 0.125.

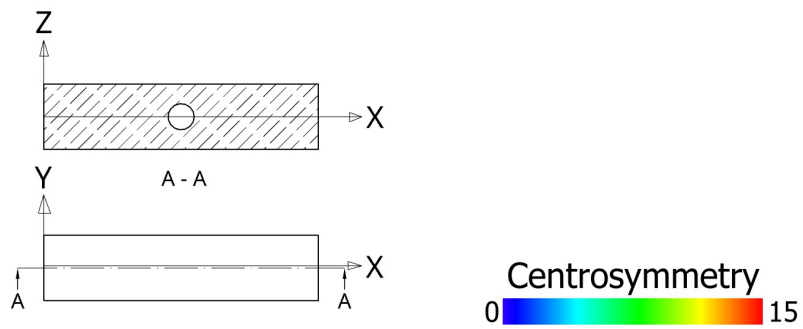


**Figure 3.19:** Deformation of tungsten without cluster in Figure 3.16, seen in cross section A-A with  $0 \leq CSP \leq 15$ .

### 3.6.3 Helium atoms in tungsten

In an attempt to simulate helium atom diffusion inside a tungsten sample, as described in the introduction, helium atoms were added to interstitial sites in a defect free sample of tungsten. The aim of the simulations is to see which impact these atoms have on the mechanical properties.

Four simulations were performed:

- Relaxation of tungsten containing randomly distributed helium atoms, to see how helium clusters are formed.
- Formation of helium blisters on a tungsten surface.
- Deformation of tungsten containing one helium cluster.
- Deformation of tungsten containing helium clusters randomly distributed over the sample.

#### 3.6.3.1 Relaxation of tungsten containing helium atoms

This simulation was carried out by randomly placing out a number of helium atoms and then run a relaxation at a certain time, in order to see how helium clusters are formed. The simulation was performed at three different temperatures, 300K, 700K and 1000K. The simulation parameters are according to Table 3.9.

**Table 3.9:** Simulation parameters.

Relaxation steps	1000000
Time step	1fs
Temperature	300K, 700K, 1000K
Lattice parameter	3.14Å
Simulation box	24x24x24 unit cells
Crystal orientation	[1 0 0]
Loading direction	[1 0 0]
Potential	EAM4
Boundary conditions	ppp
Statistical ensemble	NPT
Strain rate	$1 * 10^8/s$
Number of helium atoms	50, 100, 200

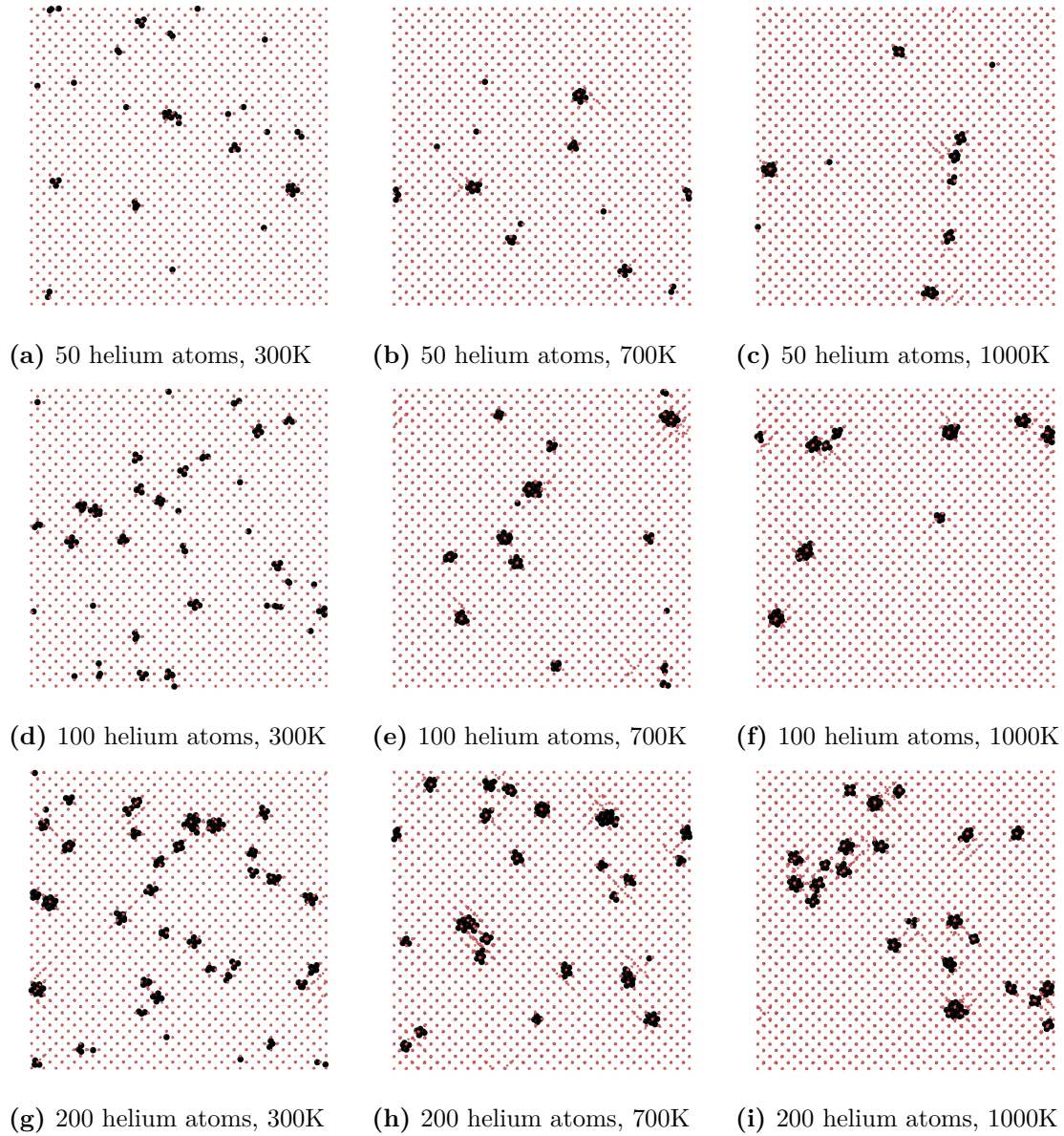


**Figure 3.20:** The structure after the relaxation process in a tungsten sample containing randomly distributed helium atoms. The red- and black dots represent tungsten and helium respectively. The simulation parameters are according to Table 3.9 .

Figure 3.20 shows that after the relaxation helium atoms gather in groups, so called helium clusters. At lower temperatures the clusters consists of just a few helium atoms, while at higher temperatures there are fewer, but larger clusters.

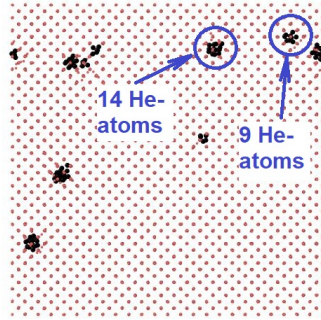
**Table 3.10:** The number of helium clusters and their mean sizes, for the tungsten samples shown in Figure 3.20.

Temp \ Helium atoms	300K	700K	1000K
50	25 2	13 3.85	11 4.55
100	36 2.78	14 7.14	11 9.09
200	46 4.35	28 7.14	23 8.7

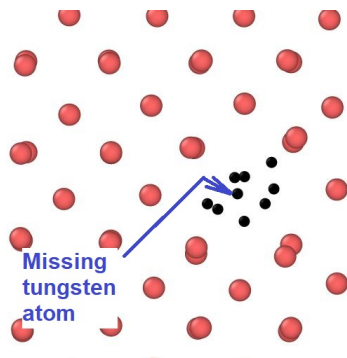
Table 3.10 shows that the mean size of the helium cluster rarely exceeds 9 atoms. In [23] it is mentioned that a single tungsten vacancy can contain at least 9 helium atoms, and that high temperature can promote the growth of helium clusters.

Figure 3.21 shows clusters both of size 9 and 14. The cluster of 9 helium atoms has taken the position of a tungsten atom.

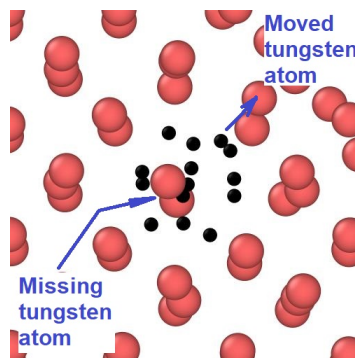




(a) 100 helium atoms, 1000K.



(b) Helium cluster of 9 surrounded by tungsten atoms.



(c) Helium cluster of 14 surrounded by tungsten atoms

**Figure 3.21:** Two sizes of helium clusters. In the first case of cluster size 9 (Figure (b)) it can clearly be seen that one tungsten atom is missing in the lattice, and 9 helium atoms have taken its place. For cluster size 14 (Figure (c)) there is also one tungsten atom missing in addition to another tungsten atom that has been pushed away a bit in order for the cluster of 14 helium atoms to fit. The black dots corresponds to the helium atoms, and the red ones to tungsten atoms.

### 3.6.3.2 Formation of helium blisters on tungsten surface

The aim of the simulation is about studying which damage a growing helium cluster inside a tungsten sample can cause on the surface. Two different temperatures will be investigated, 700K and 1500K. One difference from earlier simulations is that now the boundary condition is pps, which means that there are two free surfaces in z-direction (bottom and top surface). In order to emulate only one free surface, two atomic layers on the bottom surface are fixed from movement. In the simulation one helium atom is added every 250 timestep inside the tungsten sample where a spherical hole of radius  $6\text{\AA}$  has been created by removing the tungsten atoms. The simulation parameters are according to Table 3.11.



**Table 3.11:** Simulation parameters.

Relaxation steps	1000000
Time step	1fs
Temperature	700K and 1500K
Lattice parameter	3.14Å
Simulation box	24x24x24 unit cells
Crystal orientation	[1 0 0]
Loading direction	[1 0 0]
Potential	EAM4
Boundary conditions	pps
Statistical ensemble	NPT
Strain rate	$1 * 10^8/s$
Number of helium atoms	Increasing with 1 He-atom for every 250 timestep

Figures 3.22 and 3.23 shows the development of growing helium clusters inside tungsten samples at different temperatures.

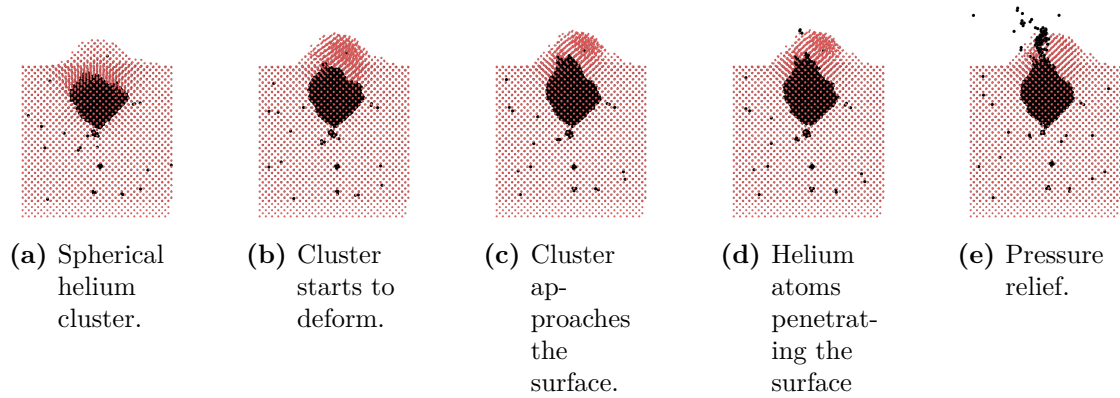


**Figure 3.22:** Formation of a helium cluster of 2600 atoms at 700K. The simulation parameters are according to Table 3.11 .

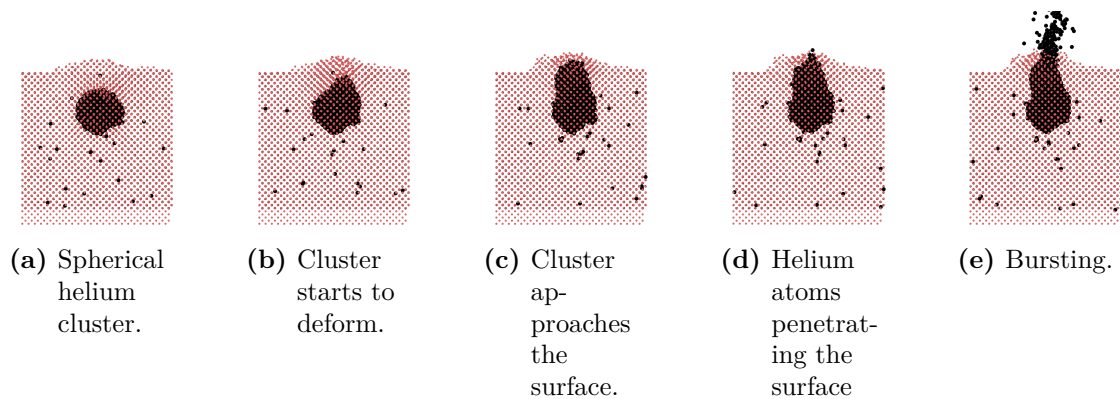


**Figure 3.23:** Formation of a helium cluster of 1480 atoms at 1500K. The simulation parameters are according to Table 3.11 .

From Figures 3.22 and 3.23 it can be seen that there is a difference in the helium cluster size between them. The pressure inside the helium bubble will be lower for the

700K simulation compared to the 1500K simulation, which causes it to burst earlier at 1500K. This means that the helium cluster when bursting will be smaller at 1500K than at 700K.

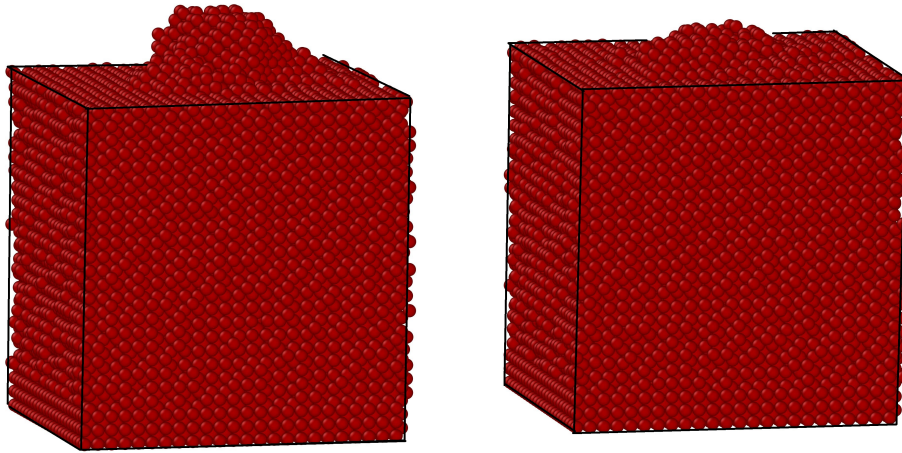


**Figure 3.24:** Comparison between surfaces after pressure relief of helium bubble. The temperature of left sample is 700K, and the right 1500K. The red spheres represent tungsten atoms.

Figure 3.24 shows the top surfaces after the pressure relief has happened. The crater formed in the left sample (700K) is larger than for the right sample (1500K), this is because the helium cluster inside this sample is larger when pressure relief happens. The tungsten atoms which are pushed away when the helium cluster is formed, are creating a hill on the free surface. The larger the helium cluster, the larger the crater. This seems to be right according to [5], who writes that when bubbles grow larger, the release of pressure occurs in a bursting event with a crater and substantial surface deformation.

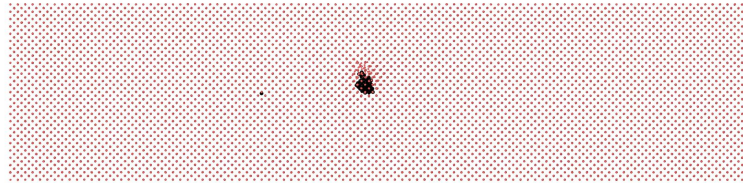
### 3.6.3.3 Deformation of tungsten containing one helium cluster.

In this simulation the goal was to see what impact helium atoms in one cluster in the middle of the sample have on the mechanical properties. The simulation parameters are according to Table 3.12.

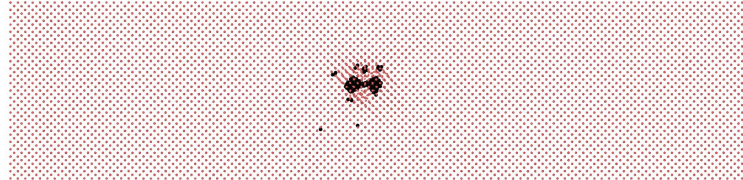
**Table 3.12:** Simulation parameters.

Relaxation steps	250000
Time step	1fs
Temperature	700K
Lattice parameter	3.14Å
Simulation box	100x24x24 unit cells
Crystal orientation	[1 0 0]
Loading direction	[1 0 0]
Potential	EAM4
Boundary conditions	ppp
Statistical ensemble	NPT
Strain rate	$1 * 10^8/s$
Number of helium atoms	75, 150, 300

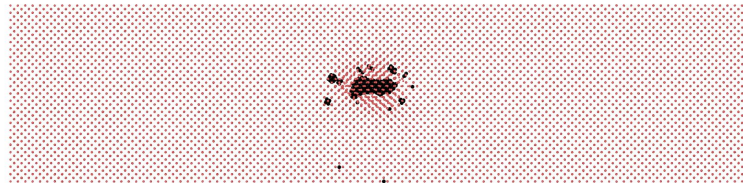
In order to ensure that a cluster was created, the helium atoms were placed close to each other at the start of the simulation. When the cluster had formed the sample looks like in Figure 3.25.



(a) Cluster of 75 helium atoms inside a tungsten sample



(b) Cluster of 150 helium atoms inside a tungsten sample



(c) Cluster of 300 helium atoms inside a tungsten sample

**Figure 3.25:** Clusters of helium atoms inside a tungsten sample, simulation parameters according to Table 3.12 . The red and black dots corresponds to tungsten and helium atoms respectively.

When looking at the stress-strain curves in Figure 3.26, one can clearly see that the helium clusters decrease both the maximum stress- and strain values. Young's mod-

ulus is only slightly affected for the clusters of 75 and 150 helium atoms, but for 300 helium atoms a sudden deterioration of this happens at a strain level of 3%. An explanation for this can be that helium clusters of this size inside a sample introduces large internal stresses, which leads to that more steps of relaxation had been needed before the tensile test simulation started. One look at the curve of cluster size 300 shows a wave-form in the start of the simulation, this is telling that the relaxation of the sample was inadequate.

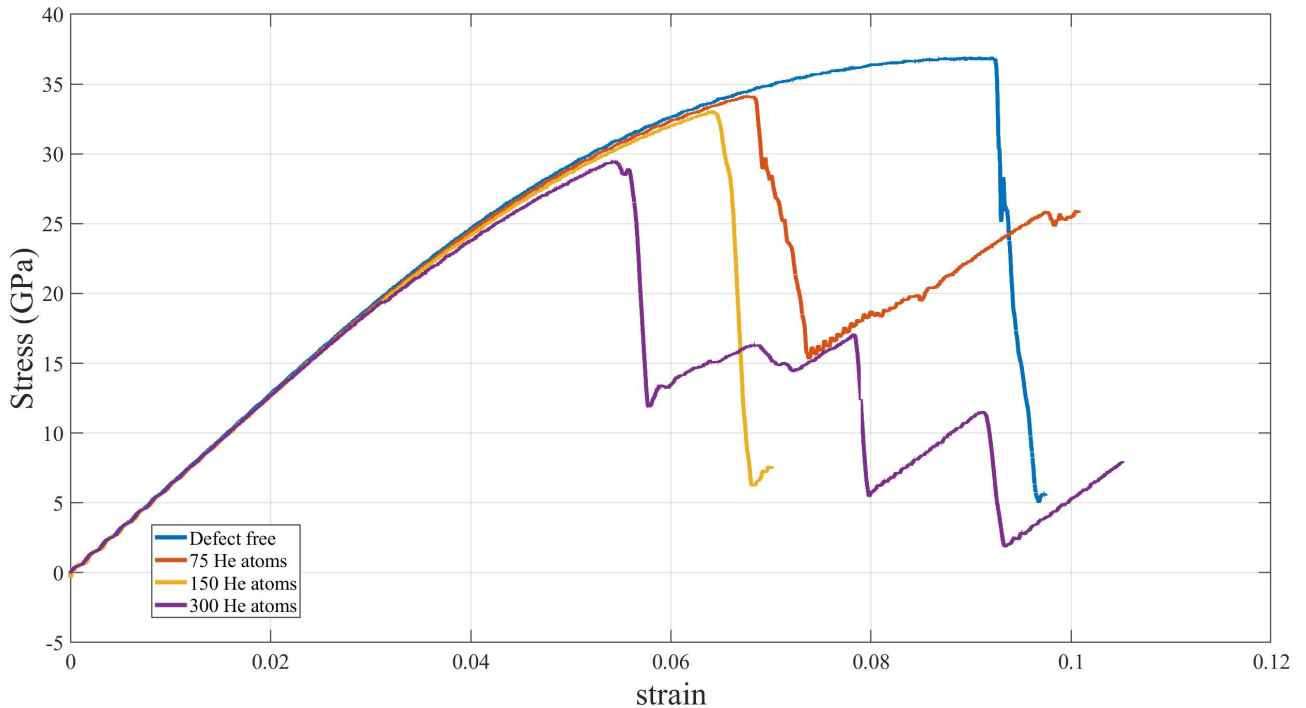
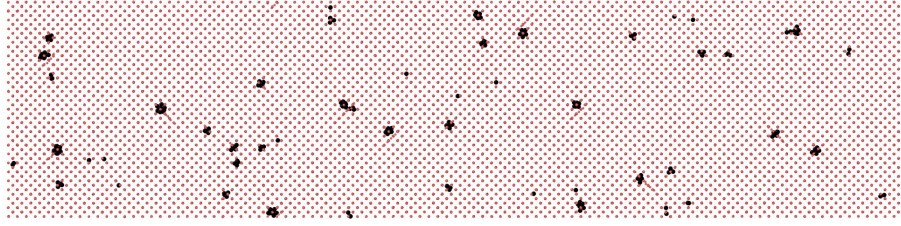


**Figure 3.26:** Stress-strain curves of helium clusters inside a tungsten sample, simulation parameters according to Table 3.12 .

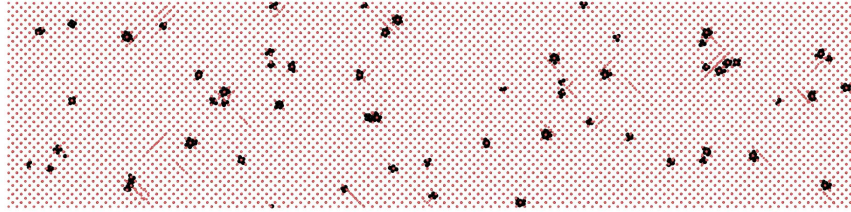
### 3.6.3.4 Deformation of tungsten containing helium clusters randomly distributed over the sample.

Here the goal is to see which impact helium atoms in several clusters in the sample have on the material properties. Helium atoms were placed randomly throughout the whole which was thereafter relaxed, after which they gathered in small clusters evenly distributed over the sample. When the clusters formed, the samples looked like in Figure 3.27.

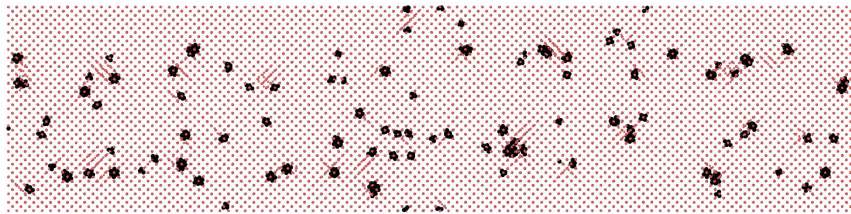




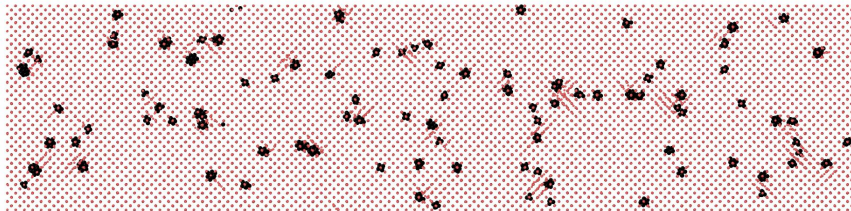
(a) 200 evenly distributed helium atoms forming small clusters inside a tungsten sample,  $T=700\text{K}$



(b) 400 evenly distributed helium atoms forming small clusters inside a tungsten sample,  $T=700\text{K}$



(c) 800 evenly distributed helium atoms forming small clusters inside a tungsten sample,  $T=700\text{K}$



(d) 800 evenly distributed helium atoms forming small clusters inside a tungsten sample,  $T=1200\text{K}$

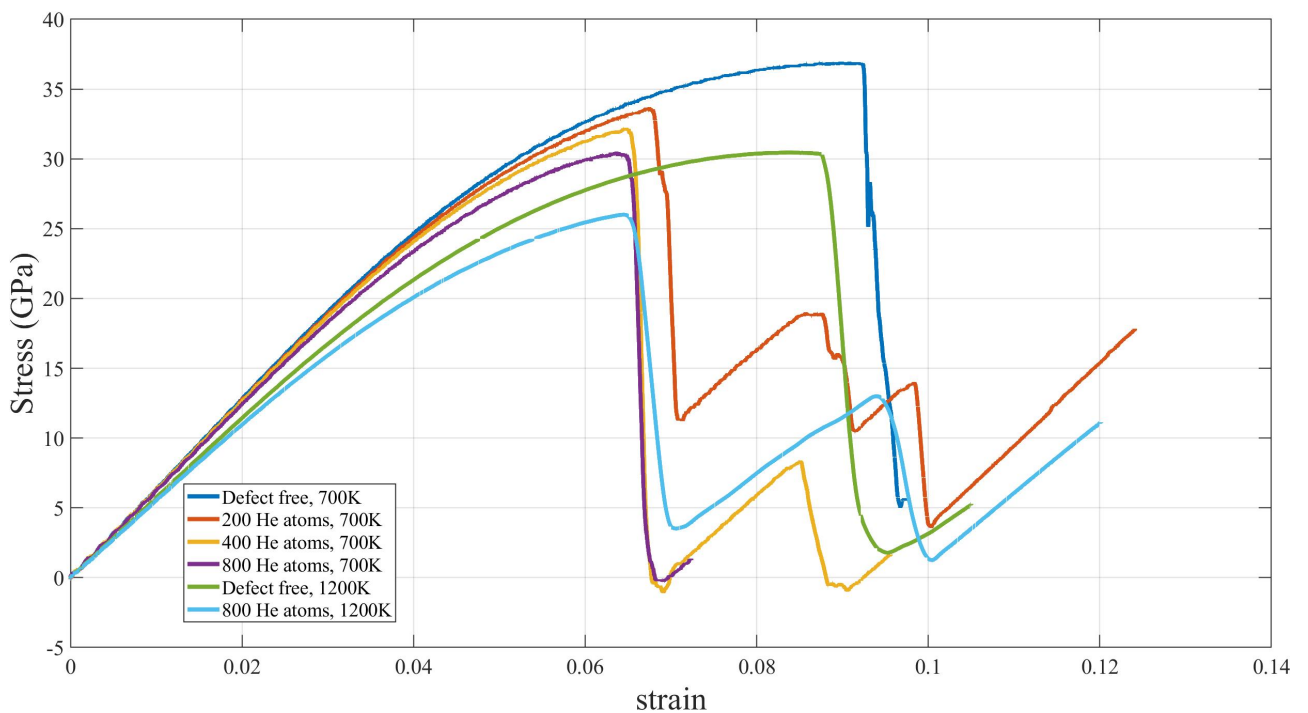
**Figure 3.27:** Helium atoms inserted in random positions in a tungsten sample, after letting the sample relax. The red and black dots corresponds to tungsten and helium atoms respectively. Simulation parameters according to Table 3.13 .

Simulation parameters are according to Table 3.13.

**Table 3.13:** Simulation parameters.

Relaxation steps	1000000
Time step	1fs
Temperature	700K and 1200K
Lattice parameter	3.14Å
Simulation box	100x24x24 unit cells
Crystal orientation	[1 0 0]
Loading direction	[1 0 0]
Potential	EAM4
Boundary conditions	ppp
Statistical ensemble	NPT
Strain rate	$1 * 10^8/s$
Number of helium atoms	200, 400, 800

When looking at the stress-strain plot in Figure 3.28 one can clearly see that the helium clusters decreased both the maximum stress- and strain values, and are affecting Young's modulus. This depends on the fact that helium clusters inside a sample introduces internal stresses, which are disadvantageous for the mechanical properties. When looking at which influence temperature has on samples containing defects of 800 helium atoms, the deterioration rate for peak stress and strain at the peak stress, is not larger at 1200K, compared to at 700K.

**Figure 3.28:** Stress-strain curves of randomly distributed helium clusters in a tungsten sample, simulation parameters according to Table 3.13 .

### 3.6.4 Combination of defects

In Figure 3.29 the stress-strain curves of samples including defects from section 3.6.1 to 3.6.3 are plotted against each other, to get an overview of the effects these have on the mechanical properties. Defects 5-7 are combinations of earlier defects.

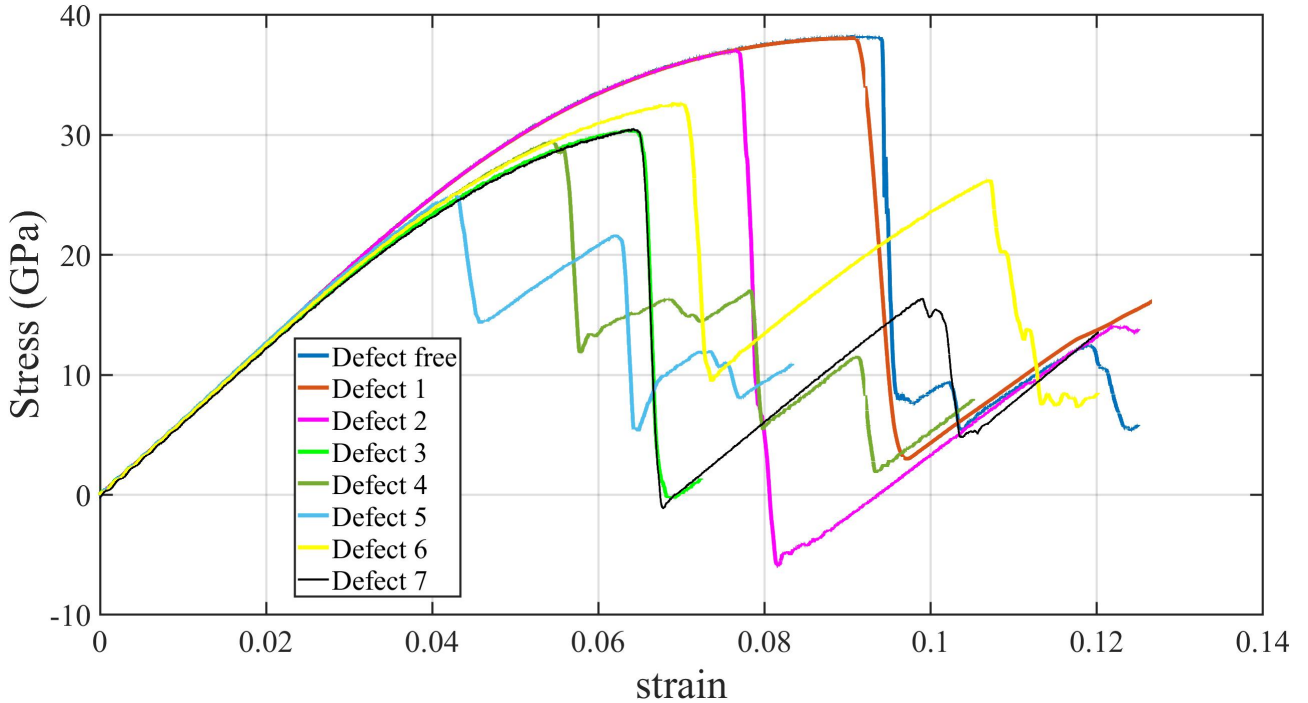


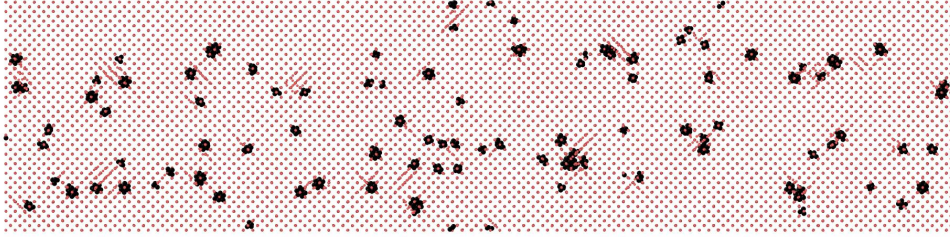
**Figure 3.29:** Stress-strains curves for samples containing different defects. 1) Vacancy density of  $10^{26}$  atoms  $/m^3$ . 2) Centrally placed vacancy cluster of size 128. 3) 800 evenly distributed He-atoms forming clusters. 4) 300 He-atoms in a centrally placed cluster. 5) 300 He-atom in centrally placed cluster with  $10^{26}$  vacancies  $/m^3$ . 6) 800 evenly distributed He-atoms forming clusters, with vacancy density  $10^{26}$  vacancies  $/m^3$ . 7) 800 evenly dist He-atoms forming clusters in combination with centrally placed vacancy cluster of size 128.

From looking at the stress-strain curves 3.29, three interesting comparisons now will be made:

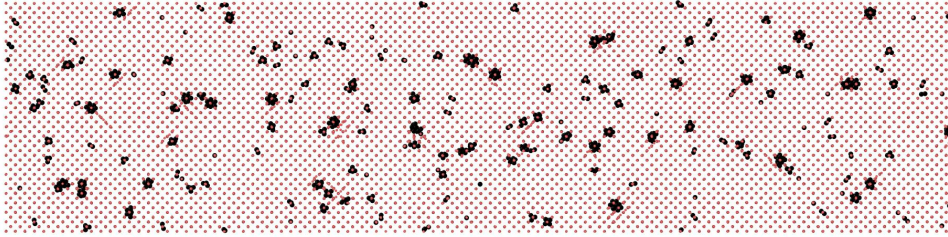
#### 3.6.4.1 Defects 3 and 6.

When comparing the two defects 3 (800 evenly distributed He-atoms forming clusters.) and 6 (800 evenly distributed He-atoms forming clusters, with vacancy density  $10^{26}$  vacancies  $/m^3$ ) seen in Figure 3.29, it seems strange that the sample without the vacancies, defect 3 shows less good mechanical properties in relation to the sample with vacancies. To illustrate why this is the case, Figure 3.30 shows pictures of the structures right after the relaxation process:





(a) Defect 3, 800 randomly distributed He-atoms forming clusters, without vacancies.



(b) Defect 6, 800 randomly distributed He-atoms forming clusters, with vacancy density  $10^{26}$  vacancies  $/m^3$ .

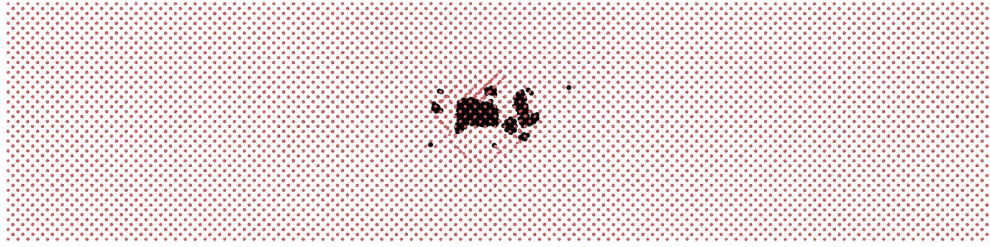
**Figure 3.30:** Clusters of helium atoms inside tungsten samples. The red and black dots corresponds to tungsten and helium atoms respectively.

Figure 3.30 shows that in the sample without vacancies, the helium clusters are fewer, but larger, than in the sample with vacancies. This can be explained by the fact that helium clusters become immobile when they are trapped by vacancies [23]. In this way the clusters are not growing as big as in the samples without vacancies, where the larger helium clusters introduce higher stresses in the sample. This explains why the sample without the vacancies does not have as good mechanical properties as the one with vacancies.

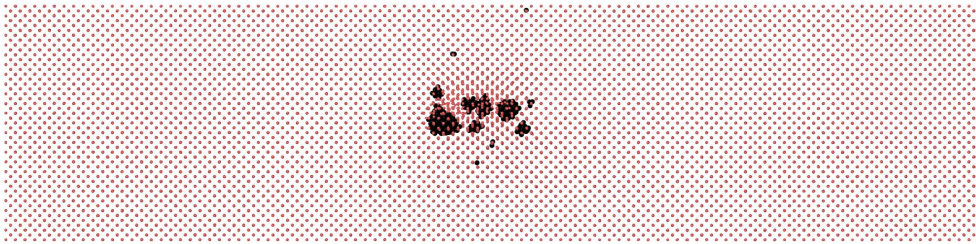
#### 3.6.4.2 Defects 4 and 5.

A comparison between defects 4 (300 He-atoms in a centrally placed cluster.) and 5 (300 He-atom in a centrally placed cluster with  $10^{26}$  vacancies  $/m^3$ ) in Figure 3.29 will now be done. Figure 3.31 shows the structure in the two different samples right after the relaxation process.





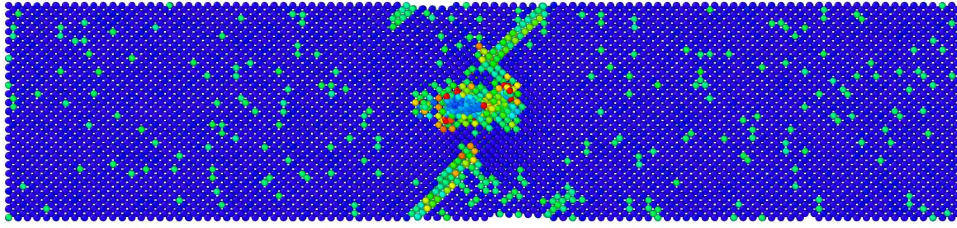
(a) Defect 4, 300 He in centrally placed cluster without tungsten vacancies.



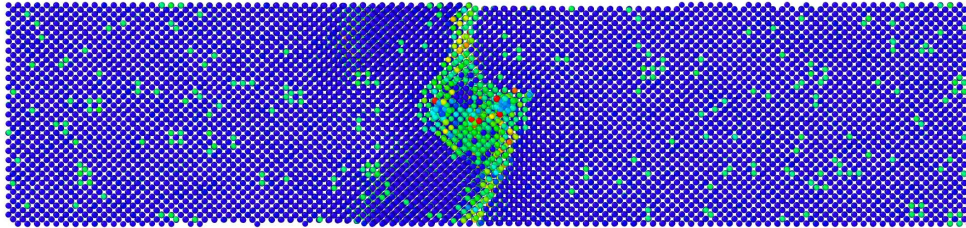
(b) Defect 5, 300 He in centrally placed cluster and  $10^{26}$  tungsten vacancies  $/m^3$ .

**Figure 3.31:** Centrally positioned clusters of helium atoms inside tungsten samples. The red and black dots corresponds to tungsten and helium atoms respectively.

As can be seen from Figure 3.31 , the helium clusters become larger in the sample without vacancies. Both samples at the top of the stress-strain curves, just before plastic deformation starts can be seen in Figure 3.32.



(a) Defect 4, 300 He in centrally placed cluster without tungsten vacancies.



(b) Defect 5, 300 He in centrally placed cluster and  $10^{26}$  tungsten vacancies  $/m^3$ .

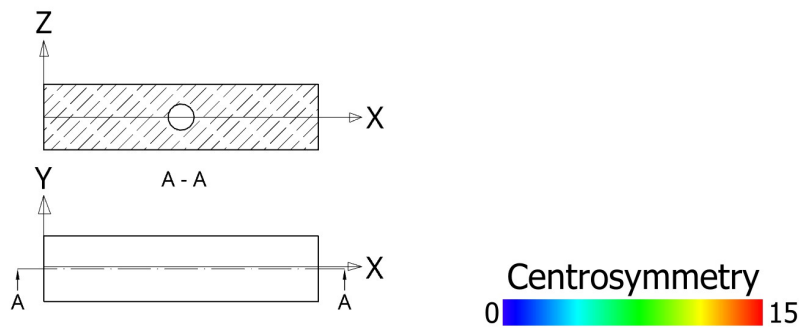


**Figure 3.32:** Centrally positioned clusters of helium atoms inside a tungsten sample. Picture taken at the top of the stress-strain curves, just before the fracture happens.

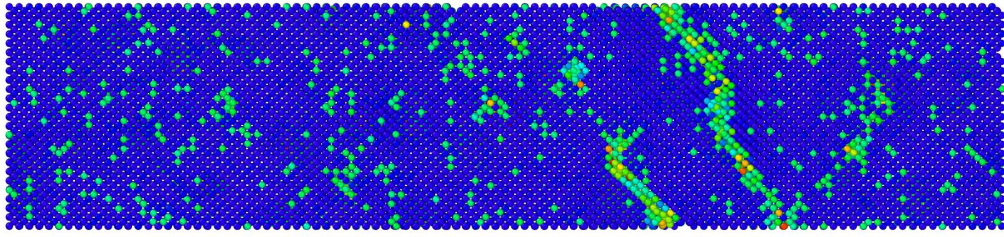
Plastic deformation in both cases starts in the position of a centrally placed helium cluster. Out of a centrally placed cluster consisting of the same number of helium atoms distributed on smaller clusters, compared to larger ones, the smaller clusters are worse for the mechanical properties. This because that a larger volume is weakened and that this leads to earlier plastic deformation for a sample with defect 5. In this simulation the position of the randomly placed vacancies should not play an important role as in section 3.6.1, where the boundary conditions were pss, unlike now, when they are ppp.

### 3.6.4.3 Defects 3 and 7.

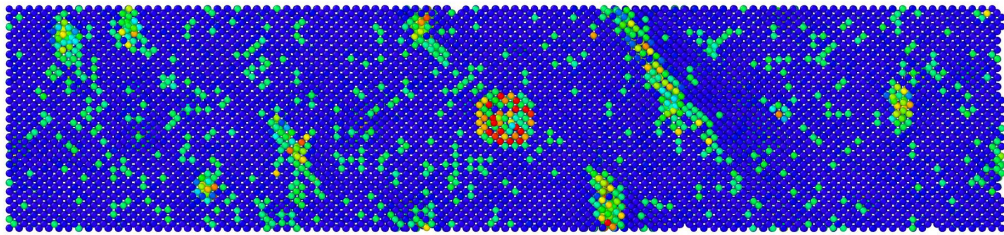
One last comparison will be made, 800 randomly distributed helium atoms with and without vacancy clusters of size 128, positioned in the middle of the sample. From Figure 3.29 it is hard to see any difference between these two. The vacancy cluster seems to have no impact on the mechanical properties when these amounts of randomly



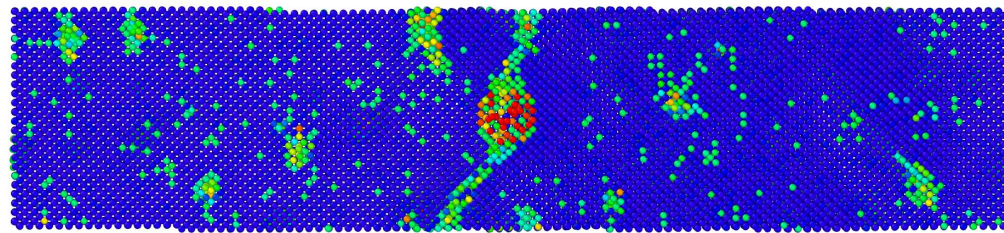
distributed helium clusters are involved.



(a) This is where the fracture starts, strain 0.065. (This view is seen without cross section.)



(b) Strain 0.065. The same picture as in a) , but with a cross section through the middle of the sample which clearly shows that the fracture does not start in the centrally placed cluster.



(c) Strain 0.06575. A cross section through the middle of the sample shows that first at this strain the fracture has reached the centrally placed cluster.

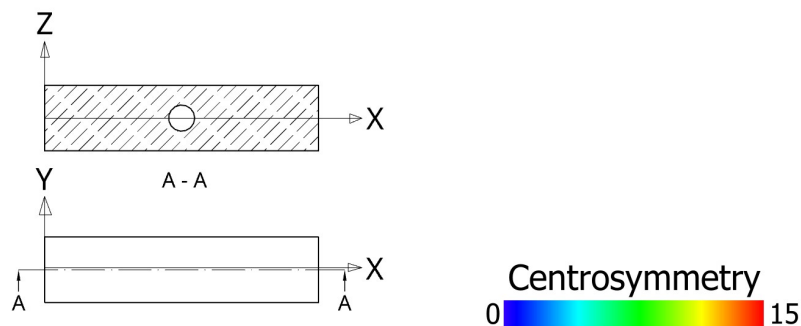


**Figure 3.33:** Defect 7, 800 evenly distributed He-atoms forming clusters in combination with centrally placed vacancy cluster size 128

When looking at the fracture development for the sample with the centrally placed vacancy cluster (Defect 7), in Figure 3.33, it can clearly be seen that the plastic deformation starts outside the vacancy cluster. From this the conclusion can be drawn that these small helium clusters are much more deteriorating on the peak stresses and

failure strains, than the vacancy clusters of size 128.

## 4 Conclusions

This work is a study of the influences that defects have on the mechanical properties of tungsten. From the performed simulations a quick summary can be made of the mechanical deteriorations caused by the defects under the current circumstances at ESS.

### **Vacancies:**

If the vacancies are within the limits specified from ESS, and the temperature is about 700K, Young's modulus will not be noticeably affected, but the peak stress and the strain at peak stress will decrease a bit. For this defect the position of the vacancy matters. If this is positioned on a surface this is worse for the mechanical properties, compared to if it is inside the sample.

For vacancy clusters the mechanical properties will be affected, the larger the vacancy cluster, the larger the decrease in the strain at peak stress. The difference in peak stress will not differ this much. There will be no change in Young's modulus.

### **Helium atoms:**

In the simulations with tungsten containing helium atoms, the statement in [23], that when a helium bubble reaches a certain size it becomes immobile, seemed to be true. It could be seen that at these temperatures the helium bubble must grow to a certain size before moving to the surface and release the pressure. This means that if the helium atoms are placed randomly and then relaxed, there are no risk for them to grow large enough to move to the surface and cause blisters. They will become immobile long before reaching the sizes that was demanded to create a blister. The only way to create a helium blister at these temperatures seems to be if the helium atoms are continuously added at the same position until the bubble bursts.

For larger helium clusters the same arguments as above applies: the risk of these to gather in one larger cluster is small at the temperature 700K.

For smaller helium clusters evenly distributed inside the tungsten sample, the deterioration of the mechanical properties can be quite large.

### **Comparison of defects:**

Since the current environment on ESS facility can lead to defects in tungsten, it would be interesting to find out which of the defects that are most likely to happen. Since the risk of large helium clusters are formed at 700K is relatively small, the simulations that contains this defect are removed. Of the remaining defects, the ones that can cause most impairment of the mechanical properties are when 800 randomly positioned helium atoms forms small clusters inside the tungsten sample. Here Young's modulus, peak stress and strain at peak stress all decreased.

The second worst defect is when a vacancy cluster of size 128 are present. This defect will not contribute to a change in Young's modulus. There will however be a quite

large decrease in strain at peak stress. The peak stress will not differ this much. The third worst defect is a vacancy density of  $10^{26}$  atoms  $/m^3$ . From the simulations it emerges that vacancies in a tungsten sample will not affect Young's modulus, but the peak stress and strain at peak stress will decrease a bit. In Figure 4.1 these comparisons are shown.

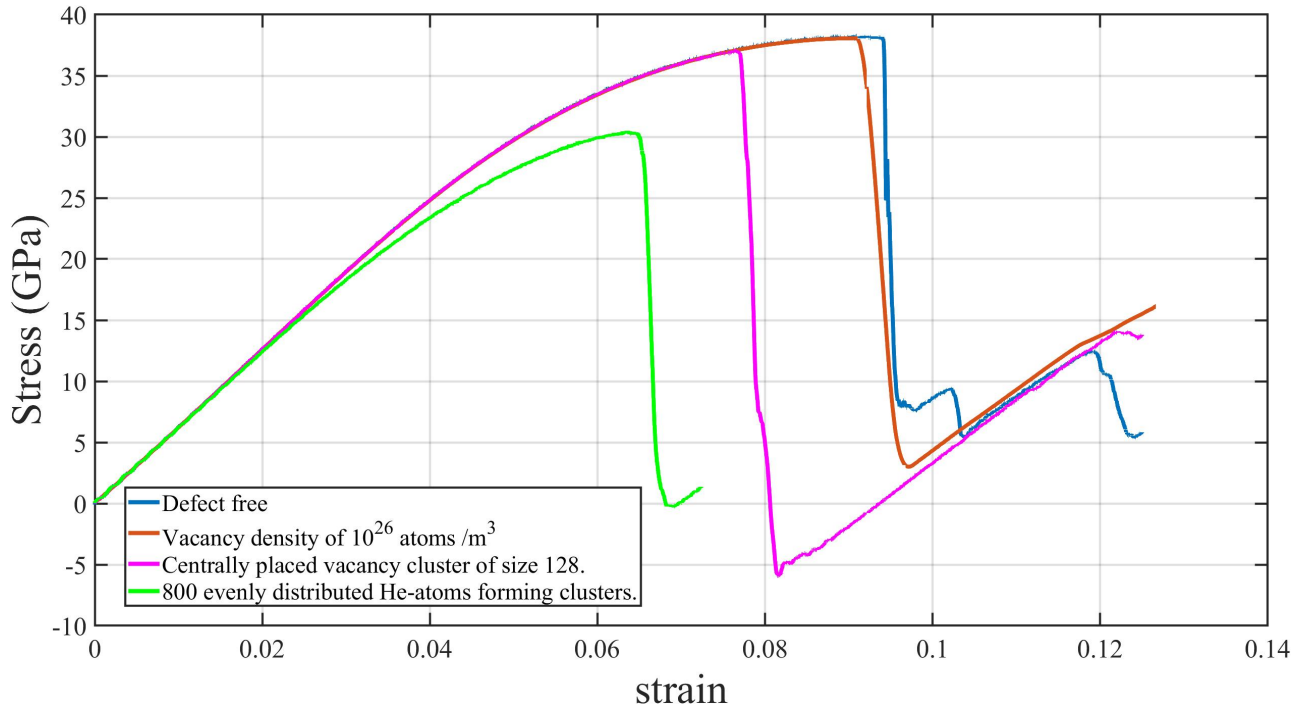


**Figure 4.1:** Stress-strain curves of defects likely to happen in the environment at ESS facility.

## 5 Recommendations for future work on the topic.

There are more defects besides the ones in this work that would have been interesting to include in the simulations, for instance dislocations and grain boundaries. Maybe look deeper into the influence of other interstitial atoms. Hydrogen is a candidate for this, it is about the same size as helium.





# Bibliography

- [1] Ventelon L. Gilbert M. Proville L. Dudarev S. Marian J. Bencteux G. Marinica M. and F Willaime. *Interatomic potentials for modelling radiation defects and dislocations in tungsten*. 2013.
- [2] Dai Y. Horvath B. and Y. Lee. *Annealing effect on the microstructure of tungsten irradiated in SINQ target*. 2018.
- [3] European Spallation Source. *Target, how it works*. Website. Accessed: 30 March 2022. 2022. URL: <https://europeanspallationsource.se/target/how-it-works>.
- [4] Perez D. Uberuaga B. Sandoval L. and A. Voter. *Formation of helium-bubble networks in tungsten*.
- [5] Juslin N. Sefta F. and B. Wirth. *Helium bubble bursting in tungsten*. 2013.
- [6] W. Callister and D. Retwisch. *Fundamentals of Materials science and engineering*. 5th ed. Hoboken, N.J.: Wiley, 2008.
- [7] Ast J. Ispánovity P. Michler J. Kalácska S. and X. Maeder. *3D HR-EBSD Characterization of the plastic zone around crack tips in tungsten single crystals at the micron scale*. 2020.
- [8] R. Smallman and R. J. Bishop. *Modern Physical Metallurgy and Materials Engineering*. 6th ed. Elsevier Science, 1999, pp. 85–89.
- [9] *Periodic Trends - Atomic Size, Ionization Energy, and Metallic Character*. [Online; accessed 2022-04-18]. 2021.
- [10] Qing Hou, Ailin Yang, Mingjie Qio, Jiechao Cui and Lei Zhai. *New insight into the diffusion of hydrogen and helium atoms in tungsten*. 2019. DOI: 10.48550/ARXIV.1912.05750. URL: <https://arxiv.org/abs/1912.05750>.
- [11] A.F. Voter. *Los Alamos Unclassified Technical Report LA-UR 93-3901*. 1993.
- [12] J.H. Westbrook A.F. Voter and R.L. Fleischer. *The Embedded Atom Method in Intermetallic Compounds: Principles and Practice*. 1994.
- [13] Gemma Safont Camprubí. “Mechanical properties at nano-level”. In: 2010.
- [14] Luca M. Ghiringhelli. *Statistical Mechanics and Molecular Dynamics*. <http://helper.ipam.ucla.edu> 2014.
- [15] J Grigera. *Molecular Dynamics Simulation for Ligand-Receptor Studies. Carbohydrates Interactions in Aqueous Solutions*. 2002.
- [16] A. P. Thompson, H. M. Aktulga, R. Berger, D. S. Bolintineanu, W. M. Brown, P. S. Crozier, P. J. in ’t Veld, A. Kohlmeyer, S. G. Moore, T. D. Nguyen, R. Shan, M. J. Stevens, J. Tranchida, C. Trott and S. J. Plimpton. “LAMMPS - a flexible simulation tool for particle-based materials modeling at the atomic, meso, and continuum scales”. In: *Comp. Phys. Comm.* 271 (2022), p. 108171. DOI: 10.1016/j.cpc.2021.108171.

- [17] Aktulga H. Berger R. Bolintineanu D. Brown W. Crozier P. in 't Veld P. Kohlmeyer A. Moore S. Nguyen T. Shan R. Stevens M. Tranchida J. Trott C. Thompson A. and S. Plimpton. *LAMMPS - a flexible simulation tool for particle-based materials modeling at the atomic, meso, and continuum scales*. 2022.
- [18] Jakob Schiøtz. *Neighbor lists*. Website. Accessed: 2 May 2022. 2022. URL: <https://wiki.fysik.dtu.dk/asap/Neighbor%20lists>.
- [19] Alexander Stukowski. “Visualization and analysis of atomistic simulation data with OVITO—the Open Visualization Tool”. In: *Model. Simul. Mater. Sci. Eng.* 18 (2010), p. 015012. ISSN: 8. DOI: 10.1088/0965-0393/18/1/015012.
- [20] Cynthia L. Kelchner, S. J. Plimpton and J. C. Hamilton. “Dislocation nucleation and defect structure during surface indentation”. In: *Phys. Rev. B* 58 (17 1998), pp. 11085–11088. DOI: 10.1103/PhysRevB.58.11085. URL: <https://link.aps.org/doi/10.1103/PhysRevB.58.11085>.
- [21] Shang J. Qin S. Lu G. Feng Y. and Y. Chen. *Twin and dislocation mechanisms in tensile W single crystal with temperature change: a molecular dynamics study*. 2018.
- [22] Z. Shen L. Gan Y. Chen Professor and H. Fang. *Hypersurface for the Combined Loading Rate and Specimen Size Effects on Material Properties*. 2005.
- [23] Guo Z. Dang W. Wang J. and D. Liu. *Molecular dynamics investigation of the configuration and shape of helium clusters in tungsten*. 2020.

# Appendix A

## Example LAMMPS script

### Description of the LAMMPS-program below

The sample size is 100x24x24 unit cells, consisting of tungsten atoms with crystal direction [1 0 0] and has a lattice parameter 3.14339Å.

The temperature is 700K.

Potential function EAM4.

Time step length 5fs.

Boundary conditions pss.

This simulation first performs a relaxation process consisting of 50000 time steps.

Thereafter it performs a tensile test where the strain rate is  $1 * 10^8/s$ . Here there are 500000 time steps. The screen output every 50 time steps will be: step number, current length, volume, temperature, stress in x-direction, strain.

```
#Defining type of atoms, dimensions and boundary conditions.
units metal
dimension 3
boundary p s s
atom_style atomic
variable latconst equal 3.14339

#Defining the lattice and creating the atoms.
lattice bcc ${latconst}
region nanowire block 0 314.339 0 75.44136 0 75.44136 units box
create_box 3 nanowire
lattice bcc ${latconst} orient x 1 0 0 orient y 0 1 0 orient z 0 0 1
create_atoms 1 region nanowire ratio 1 124546

#Defining the mass and atomic potential
mass * 183.84
pair_style eam/fs
pair_coeff * * w_eam4.fs WWW

##### RELAXATION PROCESS #####

#Creating initial velocities.
velocity all create 700 511124 rot yes mom yes
```

```

#Defining timeintegration , ensemble and temperature.
fix 1 all npt temp 700 700 0.1 x 0 0 100

# Store final cell length for strain calculations
variable tmp equal "lx"
variable L0 equal ${tmp}
print "Initial Length, L0: ${L0}"

#Compute the stress for each atom and sum each component for all atoms
compute peratom all stress/atom NULL
compute sigmaxx all reduce ave c_peratom[1]

#Create a variable called strain , which calculates the strain.
variable strain equal (lx-v_L0)/v_L0

# Screen output
thermo 50
thermo_style custom step lx vol temp c_sigmaxx v_strain
dump 1 all atom 500 dump.all
dump_modify 1 append yes

#Defining the timestep and number of timesteps.
timestep 0.005
run 50000

unfix 1

##### DEFORMATION PROCESS #####

#Defining strain rate.
fix 9 all deform 1 x vel 0.0314339 units box

#Defining timeintegration , ensemble and temperature.
fix 6 all nvt temp 700 700 0.1

#Defining the number of timesteps
run 500000

print "All done"

```